

1 **Identifying Human Specific Adverse Outcome Pathways of Per- and**
2 **Polyfluoroalkyl Substances Using Liver-Chimeric Humanized Mice**

3
4 Dakota R. Robarts¹, Diego Paine-Cabrera¹, Manasi Kotulkar¹, Kaitlyn K. Venneman¹,
5 Sumedha Gunewardena², J. Christopher Corton³, Christopher Lau⁴, Lander Foquet⁵,
6 Greg Bial⁵, and Udayan Apte¹

7
8 ¹Department of Pharmacology, Toxicology, and Therapeutics, University of Kansas
9 Medical Center, Kansas City, KS

10 ²Department of Molecular and Integrative Physiology, University of Kansas Medical
11 Center, Kansas City, KS

12 ³Center for Computational Toxicology and Exposure, Office of Research and
13 Development, U.S. EPA, Research Triangle Park, NC

14 ⁴Center for Public Health and Environmental Assessment, Office of Research and
15 Development, US EPA, Research Triangle Park, NC

16 ⁵Yecuris Corporation, Tualatin, OR

17
18 **Running Title:** FRG Humanized Mice as a model to study Per- and Polyfluoroalkyl
19 Substances

20
21 **Corresponding Author:**

22 Udayan Apte, PhD, DABT

23 Department of Pharmacology, Toxicology, and Therapeutics

24 University of Kansas Medical Center

25 3901 Rainbow Blvd., MS1018

26 Kansas City, KS 66160

27 Tel: (913) 588-9247

28 E-mail: uapte@kumc.edu

29 **Keywords:** PFAS, Humanized mice, PFOA, PFOS, GenX, RNA-Seq, Circadian rhythm

30
31 **Declaration of conflicts of interest:** LF and GB are employed by Yecuris Corp., the
32 company that sells FRG humanized mice. All other authors declare that they have no
33 actual or potential competing financial interests. This study has been subjected to
34 review by the Center for Computational Toxicology and Exposure, Office of Research
35 and Development, EPA and approved for publication. Approval does not signify that the
36 contents reflect the views of the Agency, nor does mention of trade names or
37 commercial products constitute endorsement or recommendation for use.

38
39 **Financial Support:** These studies were supported by NIH-COBRE (P20 RR021940-03,
40 P30 GM118247, P30 GM122731), NIH S10 OD021743, NIH R01 DK0198414, and NIH
41 R56 DK112768

42

43 **Abstract**

44 **Background** Per- and polyfluoroalkyl substances (PFAS) are persistent organic
45 pollutants with myriad adverse effects. While perfluorooctanoic acid (PFOA) and
46 perfluorooctane sulfonic acid (PFOS) are the most common contaminants, levels of
47 replacement PFAS, such as perfluoro-2-methyl-3-oxahexanoic acid (GenX), are
48 increasing. In rodents, PFOA, PFOS, and GenX have several adverse effects on the
49 liver, including nonalcoholic fatty liver disease. **Objective:** We aimed to determine
50 human-relevant mechanisms of PFAS induced adverse hepatic effects using FRG liver-
51 chimeric humanized mice with livers repopulated with functional human hepatocytes.
52 **Methods:** Male humanized mice were treated with 0.067 mg/L of PFOA, 0.145 mg/L of
53 PFOS, or 1 mg/L of GenX in drinking water for 28 days. Liver and serum were collected
54 for pathology and clinical chemistry, respectively. RNA-sequencing coupled with
55 pathway analysis was used to determine molecular mechanisms. **Results:** PFOS
56 caused a significant decrease in total serum cholesterol and LDL/VLDL, whereas GenX
57 caused a significant elevation in LDL/VLDL with no change in total cholesterol and HDL.
58 PFOA had no significant changes in serum LDL/VLDL and total cholesterol. All three
59 PFAS induced significant hepatocyte proliferation. RNA-sequencing with alignment to
60 the human genome showed a total of 240, 162, and 619 differentially expressed genes
61 after PFOA, PFOS, and GenX exposure, respectively. Upstream regulator analysis
62 revealed inhibition of NR1D1, a transcriptional repressor important in circadian rhythm,
63 as the major common molecular change in all PFAS treatments. PFAS treated mice had
64 significant nuclear localization of NR1D1. *In silico* modeling showed PFOA, PFOS, and
65 GenX potentially interact with the DNA-binding domain of NR1D1. **Discussion:** These
66 data implicate PFAS in circadian rhythm disruption via inhibition of NR1D1. These
67 studies show that FRG humanized mice are a useful tool for studying the adverse
68 outcome pathways of environmental pollutants on human hepatocytes in situ.

69 Introduction

70 Per- and polyfluoroalkyl substances (PFAS) are a class of anthropogenic compounds
71 used in a variety of products (Lindstrom et al. 2011). The stability of the fluorinated
72 carbon backbone of these compounds gives them extraordinary water and stain
73 resistance but also makes them non-biodegradable, leading to environmental
74 persistence (Kurwadkar et al. 2022; Rahman et al. 2014). PFAS environmental
75 contamination is of significant concern because of the numerous adverse health effects
76 induced by these chemicals. PFOA and PFOS are the two most abundant PFAS found
77 in the environment (Domingo and Nadal 2019). In humans, both PFOA and PFOS have
78 long half-lives and show substantial bioaccumulation (Fu et al. 2016; Li et al. 2018; Xu
79 et al. 2020). While both PFOA and PFOS have been phased out of production in the
80 United States (US), they are still being imported into the US (Brennan et al. 2021;
81 Sunderland et al. 2019). In recent times, the use of new 'replacement' short-chain PFAS
82 with shorter half-lives and lower bioaccumulation such as perfluoro-2-methyl-3-
83 oxahexanoic acid (GenX) has increased (Sunderland et al. 2019). Our recent studies
84 have shown that GenX is potentially hepatotoxic to humans (Robarts et al. 2022b),
85 consistent with previous rodent studies (Chappell et al. 2020; Guo et al. 2021). GenX
86 has been detected in the Cape Fear River Basin in North Carolina and the Rhine River
87 in the Netherlands (Gebbink and van Leeuwen 2020; Guillette et al. 2020; Hopkins et al.
88 2018; Moller et al. 2010). These rivers are sources of drinking water for multiple cities,
89 increasing the possibility of human exposure.

90
91 Human epidemiology studies show that PFAS exposure is associated with adverse
92 hepatic effects, including hypercholesterolemia, changes in bile acid composition, and
93 promotion of non-alcoholic fatty liver disease (NAFLD) (Fenton et al. 2021; Sen et al.
94 2022; Steenland et al. 2009). The majority of studies identifying PFAS-induced adverse
95 outcome pathways (AOPs) in the liver have been carried out in rodents. These studies
96 suggest that activation of the nuclear receptor peroxisome proliferator-activated
97 receptor alpha (PPAR α) by PFOA, PFOS, GenX, and other PFAS is the primary
98 mechanism of action in rodents (Chappell et al. 2020; Rosen et al. 2017). The human
99 relevance of PPAR α activation as a mechanism of action underlying
100 hepatocarcinogenicity has been questioned (Corton et al. 2018; Klaunig et al. 2003).
101 Patients who received fenofibrate (a PPAR α agonist) treatment for hyperlipidemia do
102 not develop hepatocellular carcinoma (HCC) (Cunningham et al. 2010; Mukherjee et al.
103 1994). This suggests that PFAS activates different key events (KEs) in rodents
104 compared to humans (Andersen et al. 2021; Corton et al. 2018; Klaunig et al. 2003).
105 There is a critical need to investigate the mechanisms of PFAS-induced hepatotoxicity
106 using more human-relevant models. Previously, other models including transgenic
107 PPAR α -knockout mice that express the human gene for PPAR α , primary human
108 hepatocytes, and human hepatic spheroids have been used to identify PPAR α -
109 independent mechanisms (Beggs et al. 2016; Reardon et al. 2021; Robarts et al. 2022b;
110 Rowan-Carroll et al. 2021; Schlezinger et al. 2021). Here, we utilized a novel *in vivo*
111 human-relevant model to study AOPs in response to PFAS exposure.

112
113 The FRG humanized mice are unique in that their livers are repopulated with
114 hepatocytes from a human liver donor (Azuma et al. 2007). Additionally, there is

115 continual genetic selection pressure to maintain the human hepatocytes, preventing
116 mouse cholangiocytes from dedifferentiation into functional mouse hepatocytes. These
117 humanized mice have been utilized as a model to study liver diseases, including
118 NAFLD, viral hepatitis, alcoholic fatty liver disease, and malaria infection (Foquet et al.
119 2018; Long et al. 2018; Ma et al. 2022; Stone et al. 2021; Tyagi et al. 2018; Wang et al.
120 2019) as well as a unique human-relevant model to study the effects of chemicals on
121 human hepatocytes *in vivo*. We hypothesize that humanize mice will identify human
122 relevant mechanisms of PFOA, PFOS, and GenX-induced hepatotoxicity.

123 **Methods**

124 *FRG Humanized Mice*

125 All animal studies were approved and performed under the Institutional Animal Care
126 and Use Committee at the University of Kansas Medical Center (KUMC). FRG KO
127 humanized mice on a NOD background that were 25-week-old were kindly provided by
128 Yecuris, Corp. Humanized mice were generated by injecting cryopreserved human
129 hepatocytes obtained from a single 18-year-old male donor in male triple transgenic
130 male mice (Fah^{-/-}, Rag^{-/-}, and Il2rg^{-/-}) and inducing repopulation of the livers (**Fig. 1A**),
131 as previously described (Azuma et al., 2007). The mice were housed in the KUMC
132 vivarium under a standard 12-hour dark and 12-hour light cycle.

134 *PFAS Exposure and Sample Collection*

135 FRG liver-chimeric humanized mice were given water containing either 0.067 mg/L of
136 PFOA, 0.145 mg/L of PFOS, or 1 mg/L GenX ad libitum for 28 days. These
137 concentrations were based on previous reports on occupational exposure of individual
138 PFAS (Beggs et al. 2016; Chang et al. 2014; Olsen et al. 2007). PFOA (Aldrich cat#
139 77262-50G, lot # BCCB6034), PFOS (Aldrich cat # 77282-10G, lot # BCCC7858), and
140 GenX (Synquest Laboratories cat # 2122-3-09, lot # 00008887) were dissolved in 0.5%
141 Tween-20 at final concentrations of 0.067 g/L, 0.145 g/L, and 1 g/L, respectively. These
142 stocks were diluted to 0.067 mg/L (PFOA), 0.145 mg/L (PFOS), and 1 mg/L (GenX) and
143 supplemented with a final concentration of 0.5% Tween-20 and 3.25% dextrose. Due to
144 that the humanized mice were acclimated to 3.25% dextrose during development,
145 dextrose was added to their drinking water as recommended by Yecuris. The control
146 group was given water containing 0.5% Tween-20 in drinking water supplemented with
147 3.25% dextrose. All mice were given a tyrosine-free (YF-10TM) diet (to prevent liver
148 repopulation with rodent hepatocytes) ad libitum, provided by Yecuris. A sample size of
149 3 were used in all experimental groups. Mice were euthanized on exposure day 28.
150 Blood was obtained from the retro-orbital sinus, allowed to clot at room temperature for
151 10 minutes, and then centrifuged at 5000 g for 10 minutes at 4°C to isolate serum.
152 Serum analyses of cholesterol (Fisher cat # 50-489-238), ALT (Fisher cat # 23-666-089),
153 glucose (Fisher cat # 23-666-286), triglycerides (Fisher cat # 23-666-410), free fatty
154 acids (Fisher cat # 50-489-265), and bile acids (Diazyme cat # DZ042A-K01) were
155 performed using kits according to the manufacturer's protocol. Livers were removed, the
156 gallbladder was separated, and then the liver was weighed to calculate liver weight-to-
157 body weight ratios. A portion of the liver was fixed in 4% formaldehyde for 48 hours,
158 followed by an additional 24 hours in ethanol, and then processed to obtain paraffin-
159 embedded tissue sections for histology. A portion of the liver was cryopreserved in an
160 optimal cutting temperature compound (OCT) for cryosectioning. All remaining liver
161 tissues were stored at -80°C for further analysis.

163 *PFAS Extraction from Serum and Liver*

164 Serum samples were used with no additional extractions. Liver samples were prepared
165 3:1 (DI water:tissue mass) and homogenized with a 10/35 PT Polytron homogenizer
166 (Brinkmann Instruments, Westbury, NY). For serum and liver homogenate (25ul) was
167 sub-aliquoted for PFAS extraction, analysis as previously described in depth (Reiner et
168 al. 2009). In brief, proteins were denatured with formic acid, precipitated with cold

169 acetonitrile, and separated by centrifugation (2000 × g for 3 min). Extracted 8 point
170 calibration curves were made using blank rat serum (Pel-Freez Biologicals) spiked with
171 PFAS appropriate for dosed (100 – 2,500 ng/ml) or control (1-100 ng/mL) serum/liver
172 homogenate measurements. Liver homogenate concentrations were corrected for 3:1
173 dilutions and serum reported as is. An aliquot of the acetonitrile supernatant was placed
174 in an HPLC vial with 2 mM ammonium acetate buffer (pH 6.5) (1:1), and the PFAS
175 concentrations were determined using UPLC–MS/MS.

176

177 *Mass Spectrometry Analysis*

178 PFAS analyses were performed using a Thermo Vanquish Horizon ultrahigh
179 performance liquid chromatograph (UPLC) coupled to a Thermo TSQ Quantis triple-
180 quadrupole (QQQ) mass spectrometer operated in negative ion mode. A reversed
181 phase separation of sample components (100 uL) occurred on a Phenomenex Gemini
182 C18, 2 mm × 50 mm, 3.0 μm silica with TMS end-capping column (Torrance, CA) at 55
183 °C. A Thermo Scientific Hypersil GOLD C18, 1.9 μm, 3 mm × 50 mm was used as a
184 delay column (Waltham, MA) as part of in-house standard practice. The sample was
185 ionized at the mass spectrometer source using electrospray negative ionization. The
186 source and MS/MS parameters were optimized for each analyte individually. Transitions
187 for all ions were observed using multiple reaction monitoring (MRM), and analyte-
188 specific mass spectrometer parameters were optimized for each compound.

189

190 *Histology, Immunohistochemistry, and Oil Red O staining*

191 Hematoxylin and eosin staining was performed as previously described on 5 μm thick
192 paraffin imbedded tissue sections (Umbaugh et al. 2022). Paraffin-embedded liver
193 sections (5 μm thick) were used for immunohistochemical analysis of FAH, PCNA, Ki67,
194 NR1D1, CLOCK, and BMAL1 (**Table S1**), as previously described (Robarts et al.
195 2022a). Flash frozen cryosections (8 μm thick) were used for Oil Red O staining, as
196 previously described (Walesky et al. 2013).

197

198 *Protein Isolation and Western Blot Analysis*

199 For each sample, 100 mg of each liver was homogenized in RIPA buffer (Thermo Fisher
200 cat # 89901) containing 1x of phosphatase and protease inhibitors (Thermo Fisher cat #
201 78427 & 78438). In addition, nuclear, and cytoplasmic fractions were generated using
202 the NE-PER™ Nuclear and Cytoplasmic Extraction kit, according to the manufacturing
203 protocol (Thermo Fisher cat # 78835). Protein concentration was measured using a
204 BCA assay (Thermo Fisher cat # 23225) as previously described (Robarts et al. 2022a).
205 To run the western blots, 100 μg of protein was loaded into each well and run as
206 previously described in depth (Robarts et al. 2022b). The primary antibodies used in this
207 study along with the specific dilution used are shown in **Table S1**. Western blots were
208 imaged and quantified using Image Studio Lite software (Version 5.2). Densitometry
209 was then normalized to the western blot loading control.

210

211 *RNA Isolation and qPCR Analysis*

212 RNA was extracted from 50 mg of the liver using Invitrogen™ TRIzol™ Reagent
213 (Thermo Fisher cat # 15596018) as previously described (Robarts et al. 2022a). The
214 RNA was reverse transcribed to cDNA and then utilized for qPCR with 100 ng of cDNA

215 per reaction, as previously described (Apte et al. 2009). The primers utilized are shown
216 in **Table S2**. All genes were normalized to the housekeeping gene (*18S* or *Gapdh*), and
217 fold changes were calculated using the standard $2^{-\Delta\Delta CT}$ method, as previously described
218 (Livak and Schmittgen 2001).

219 220 *RNA-Sequencing*

221 Quality of RNA isolated was assessed using the Agilent TapeStation 4200. All samples
222 had an RNA integrity number equivalent (RIN^e) value greater than 9.0. cDNA libraries (n
223 of 3 per group) were generated using RNA using the Tecan Universal Plus mRNA-seq
224 kit. These libraries were then sequenced on the NovaSeq 6000 Sequencing System at
225 a sequencing depth of 25 million reads, with 100 cycle base pair paired-end read
226 resolution, provided by the University of Kansas Genomics Core, as previously stated
227 (Gunewardena et al. 2022). An online PFAS dataset using human spheroids as a model
228 was downloaded using SRA-tools from the GEO database, which was analyzed in
229 parallel to the humanized mice RNA-Seq dataset (GSE144775) (Rowan-Carroll et al.
230 2021). Raw fastq files were then aligned to the human genome (GRCh38), and genes
231 were counted using STAR software (Version 2.3.1u) (Dobin et al. 2013) run on an HPE
232 DL380 Gen10 8SFF CTO high-performance server. The counts were then normalized
233 using the median of ratio method, and differentially expressed gene (DEG) lists were
234 generated using the DESeq2 package (Version 1.28.1) in R Studio (Version 4.0.3,
235 RStudio Team). For the humanized mice study, the samples were compared to the
236 control group. The raw data and normalized data generated were deposited in the GEO
237 database (GSE208636).

238 239 *Ingenuity Pathway Analysis*

240 Differentially expressed genes (DEGs) from the humanized mice (p-value < 0.05 and an
241 |foldchange| ≥ 1.5) for each treatment group were uploaded into the Qiagen Ingenuity
242 Pathway Analysis (IPA) software as previously described (Gunewardena et al. 2022;
243 Robarts et al. 2022a). The upstream regulators were then exported from the software
244 using the graphical user interface. Once exported, this dataset was uploaded to RStudio
245 (Version 4.0.3, RStudio Team). The R package ggplot2 (Version 3.3.3) was used to
246 generate dot plots, where size represents the number of genes changed in that
247 pathway, color represents the $-\log_2(\text{p-value})$, and the x-axis illustrates the z-score
248 assigned by the IPA.

249 250 *BaseSpace Correlation Engine*

251 Illumina's BaseSpace Correlation Engine (BSCE, Version 2.0) was used to determine
252 the correlation between the humanized dataset and the human spheroid dataset. Both
253 datasets were uploaded to BSCE using their online interface
254 (<https://www.basespace.illumina.com>). Briefly, BSCE uses the Running Fisher test to
255 establish positive or negative correlations with corresponding $-\log(\text{p-values})$, as
256 previously described in depth (Kupersmidt et al. 2010). These data were imported into
257 RStudio (Version 4.0.3, RStudio Team). The $-\log(\text{p-values})$ were assigned a direction;
258 for example, if there was a negative correlation, the $-\log(\text{p-value})$ was multiplied by -1.
259 The correlation $-\log(\text{p-values})$ for GenX-, PFOA-, PFOS-exposed humanized mice were

260 plotted using the R package ggplot2 (Version 3.3.3) to produce line charts and
261 heatmaps.

262

263 *in silico Docking*

264 To determine the interaction of PFOA, PFOS, or GenX with the nuclear receptor
265 NR1D1, we utilized AutoDock Vina (Trott and Olson 2010). The PDB file for NR1D1
266 (1GA5) was loaded into AutoDock Tools (Version 1.5.6) (Sierk et al. 2001). All ligands
267 and DNA were first deleted from the PDB file. Then, polar hydrogens and Gastereiger
268 charges were added along with the construction of the docking grid (90 × 102 × 110 Å)
269 (Morris et al. 2009). The chemical 3D structures of PFAS were downloaded from
270 PubChem and converted into a PDB format in PyMol (Version 4.6). The PFAS PDBs
271 were prepared using AutoDock Tools (Version 1.5.6) (Adams et al. 2010). The
272 compound was then docked using Vina, as previously described (Akakpo et al. 2019).
273 The interaction of each PFAS with NR1D1 was visualized in PyMol (Version 4.6).

274

275 *Graphs and Statistical Analysis*

276 Heatmaps, volcano plots, Venn diagrams, dot plots, and line graphs were produced in R
277 studio (Version 4.0.3, RStudio Team), as previously described using the packages
278 gplots (Version 3.1.1), RcolorBrewer (Version 1,1-2), ggVennDiagram (Version 1.1.1),
279 and ggplot2 (Version 3.3.3) (Gunewardena et al. 2022; Robarts et al. 2022a). Bar
280 graphs and statistical analyses were produced in GraphPad Prism 8. If two groups were
281 being compared, a two-tailed t-test was performed. If three or more groups were
282 compared, an ANOVA was used followed by a Tukey multiple comparison post-hoc test.
283 Statistical significance was considered when the p-value was <0.05.

284 **Results**

285 *Generating a human-relevant model to study the AOPs of PFAS.*

286 To determine the extent of retention of human hepatocytes during the 28-day exposure,
287 we performed immunohistochemistry (IHC) of the enzyme fumarylacetoacetate (FAH),
288 which is expressed only by the transplanted human hepatocytes, on the liver sections of
289 FRG mice (**Fig. 1B**). In all groups, FAH was expressed throughout the entire liver
290 lobule, indicating successful retention and an adequate number of human hepatocytes
291 (**Fig. 1B**). Next, we determined the serum and liver concentrations of PFAS using mass
292 spectrometry. The average serum concentration was 4.04 µg/mL for GenX, 2.74 µg/mL
293 for PFOA, and 4.48 µg/mL for PFOS (**Fig. 1C**). PFAS were not detected in the control
294 mice. This indicates that both PFOA and PFOS levels were in the same magnitude of
295 observed in occupational workers (0.07-5.10 µg/mL and 0.14-3.50 µg/mL, respectively)
296 (Beggs et al. 2016; Chang et al. 2014; Olsen et al. 2007). GenX levels were comparable
297 to those of PFOS. Further, all PFAS accumulated in the liver, with PFOS at the highest
298 concentration of 5.35 µg/mg followed by PFOA at 1.07 µg/mg (**Fig. 1D**). GenX had the
299 lowest amount of hepatic accumulation at 0.58 µg/mg (**Fig. 1D**). Hematoxylin and Eosin
300 (H&E) staining showed mild to moderate steatosis in the livers of all PFAS treated mice
301 with PFOA treatment showing the highest accumulation of fat (**Fig. 1E**).

302

303 *PFAS altered LDL/VLDL, bile acids, and lipid deposition in the liver.*

304 The liver-weight-to-body-weight ratio did not indicate any PFAS-related changes over
305 the control group (**Fig. 2A**). Serum ALT, a marker of liver injury, and other metabolic
306 markers, including serum glucose, triglycerides, and free fatty acids, showed no
307 significant difference between any treatment groups (**Fig. 2B-E**). Previous studies have
308 shown that serum cholesterol levels are elevated in humans exposed to PFAS
309 (Andersen et al. 2021; Frisbee et al. 2010; Steenland et al. 2009). We measured total
310 cholesterol, LDL/VLDL and HDL in the serum of the humanized mice following PFAS
311 treatment (**Fig. 2F**). Total cholesterol was similar in PFOA and GenX treated mice but
312 was significantly lower in PFOS treated mice. PFOS also caused a significant decrease
313 in LDL/VLDL compared to the control, GenX, and PFOA groups. Furthermore, GenX
314 showed a significant increase in LDL/VLDL compared to the control group (**Fig. 2G**).
315 However, PFAS-induced changes in HDL did not reach statistical significance, although
316 a trend of decreased HDL was noted in the PFOA and GenX treatment group (**Fig. 2H**).

317

318 PFAS exposure in humans has been strongly correlated with alterations in bile acids in
319 the serum (Sen et al. 2022). We measured bile acids in serum of humanized mice
320 exposed to PFOA, PFOS, and GenX and found significantly elevated bile acids in GenX
321 and PFOS treated mice (**Fig. 2I**). We performed Oil Red O staining to visualize lipid
322 accumulation, which showed significant lipid accumulation following PFOA treatment
323 (**Fig. 2J**). Interestingly, GenX had less lipid accumulation compared to the control
324 group, and PFOS showed no difference.

325

326 *PFAS induced hepatocyte proliferation in humanized mice after 28 days of exposure.*

327 To determine the extent of PPAR α in mouse and human derived hepatocyte, species
328 specific qPCR was performed. This showed an induction in mouse PPAR α target genes
329 whereas human had no change in gene expression in PFOA, PFOS, and GenX

330 treatments (**Fig. S1A-C**). To investigate whether PFOA, PFOS, or GenX treatment
331 resulted in the induction of cell proliferation in humanized mice, we performed IHC for
332 PCNA and Ki67. PFOA and PFOS caused a significant induction of cell proliferation
333 compared to the control (**Fig. 3A-C**), but GenX treatment did not cause significant
334 proliferation. Consistently, qPCR analysis showed significant induction in cyclin D1, the
335 major cell cycle regulator, in PFOA and PFOS treated mice with no change in the GenX
336 treated mice compared to the control (**Fig. 3D**). Further, western blot analysis showed
337 an induction of cyclin D1 and p-Rb proteins in the livers of PFOA, PFOS, and GenX
338 treated mice (**Fig. 3E**).

339
340 *Significant transcriptome changes were exhibited in the livers of humanized mice*
341 *exposed to PFAS.*

342 To determine the global effect of human-relevant PFAS exposures on humanized mice,
343 we performed bulk RNA-sequencing (RNA-Seq). Livers of FRG humanized mice have
344 over 80% human hepatocytes, but all the non-parenchymal cells (NPCs) are of mouse
345 origin. To determine specific changes in human hepatocytes and exclude changes
346 occurring in mouse NPCs, all alignments were performed on the human genome. We
347 compared ligand-binding nuclear receptors from human RNA-Seq datasets to
348 humanized mice RNA-Seq using a rank-based method and found that the top
349 expressed receptors were RXR α , PPAR α , and AR, whereas the least expressed
350 receptor was RXR γ (**Fig. S2A**). Cluster analysis shows that transcriptomic changes
351 following PFOA and PFOS were similar to each other but distinct from those induced by
352 GenX (**Fig. S2B**). A global analysis of all differentially expressed genes (DEGs) found
353 that PFOA caused significant downregulation of 154 genes and significant upregulation
354 of 86 genes, with the top altered genes including *KRT23*, *NRN1*, *RGS2*, *MRC2*, and
355 *UCP2* (**Fig. 4A, Table 1**). PFOS treatment downregulated 120 genes and upregulated
356 42 genes. *HSPA6*, *GRIP2*, *KRT25*, *ECEL1*, and *RASGRP2* were the top altered genes
357 after PFOS treatment (**Fig. 4B, Table 1**). GenX caused the greatest number of gene
358 changes; 446 genes were downregulated, and 173 genes were upregulated (**Fig. 4C**).
359 The top 5 DEGs after GenX treatment were *KIF18A*, *MRC2*, *PLXNA4*, *SLITRK3*, and
360 *ADAMTS1* (**Table 1**). Venn diagrams of DEGs across chemicals showed that GenX
361 uniquely upregulated 119 and uniquely downregulated 310 genes, PFOA caused
362 upregulation of 45 and downregulation of 49 unique DEGs whereas PFOS caused
363 upregulation of 9 and downregulation of 42 unique DEGs (**Fig. 4D-E**). A total of 12
364 DEGs were commonly upregulated across all PFAS groups, including *COL6A2*,
365 *MYO16*, *LAMC3*, and a variety of metallothionein genes (**Fig. 4D-E, Table 2**). In
366 addition, 23 DEGs were commonly downregulated across all exposures, including
367 *CYP3A7*, *SCL7A10*, *MRC2*, and cyclins A2 and B1 (**Fig. 4D-E, Table 3**). To visualize
368 alterations in cytochrome P450s and phase 2 drug metabolism enzymes (DMEs),
369 heatmaps were made using the fold change values when compared to the control group
370 (**Fig. S2C-B**). *CYP2A7*, *CYP3A4*, *CYP2A13*, *CYP26A1*, and *UGT1A3* were the most
371 commonly induced DMEs (**Fig. S2C-D**).

372
373 Next, to compare these *in vivo* data to *in vitro* data, we compared the humanized mice
374 DEGs of PFOA and PFOS with an RNA-Seq dataset derived from human hepatic
375 spheroids treated with either PFOA or PFOS at multiple concentrations (PFOA: 0.02,

376 0.1, 0.2, 1, 2, 10, 20, 50, or 100 μM , and PFOS: 0.02, 0.1, 0.2, 1, 2, 10, or 20 μM) and
377 time points (1-, 4-, 10-, or 14-day) (Rowan-Carroll et al. 2021). We found that our PFOS
378 treated humanized mice were most similar to the 1 μM treatment for 14 days and the
379 most different to the 2 μM treatment for 1 day (**Fig. S3A-B**). The PFOA treated mice
380 were most similar to the 14-day spheroid exposure at the 10 μM concentration (**Fig.**
381 **S3A, S2C**). Interestingly, we found that GenX was most similar to the PFOA spheroids
382 treated at the 10 μM for 10 days and most dissimilar to the PFOS 1-day exposure at 2
383 μM (**Fig. S3A**).

384
385 To provide insight into mechanisms that were contributing to these DEGs altered in
386 PFOA, PFOS, and GenX exposed mice, we uploaded the DEGs into the Ingenuity
387 Pathway Analysis (IPA) software to determine altered upstream regulators. We found
388 that PFOA significantly inhibited androgen receptor (AR), FOXM1, and NR1D1, and
389 induced activation of TP53, PPAR α , and the proinflammatory regulators INF γ and IL1B
390 (**Fig. 4F**). PFOS had the fewest total altered upstream regulators; PFOS significantly
391 inhibited FOXM1, IL6, IL1B, and NR1D1, and activated TP53 and SREBF1 (**Fig. 4G**).
392 GenX had the most significantly altered upstream regulators. GenX inhibited ESR1,
393 RAF1, NR1D1, and TAL1 and activated TP53, PPAR α , and RB1 (**Fig. 4H**).

394
395 *NR1D1 is significantly disrupted in PFAS exposed humanized mice.*

396 An interesting *in vivo* pathway was identified in the IPA analysis. The nuclear receptor
397 NR1D1 (also known as Rev-Erba) was predicted to be significantly inhibited in PFOA,
398 PFOS, and GenX treated humanized mice (**Fig. 4F-H**). NR1D1 is a nuclear receptor
399 critical for regulating circadian rhythm at the molecular level. Two circadian
400 transcriptional activators, CLOCK, and BMAL1, heterodimerize to activate a plethora of
401 genes, including NR1D1. The upregulation of NR1D1 initiates the negative feedback
402 loop that occurs during the light cycle. Once translated into protein, NR1D1 translocates
403 to the nucleus, binds to the promoter of BMAL1, and represses BMAL1 expression. This
404 causes the intracellular levels of NR1D1 to drop to restart the cycle of regulating
405 circadian rhythm (Tahara and Shibata 2016).

406
407 To investigate the disruption of NR1D1, we first performed qPCR on genes regulated by
408 CLOCK and BMAL1, including *NR1D1*, *CRY2*, *PER2*, and *PER1*. *NR1D1*, *CRY2*, and
409 *PER2* were all significantly upregulated in GenX, PFOA, and PFOS exposed humanized
410 mice (**Fig. 5A**). *PER1* was significantly elevated in the PFOA and PFOS exposed mice
411 but not in GenX treated mice (**Fig. 5A**). Western blot analysis showed a significant
412 induction of NR1D1 in all treatment groups compared to the control group, with the
413 strongest induction following GenX treatment (**Fig. 5B-C**). CLOCK protein expression
414 did not change, as expected, because NR1D1 does not regulate CLOCK expression
415 (**Fig. 5B-C**). BMAL1 protein showed no significant changes in all treatment groups (**Fig.**
416 **5B-C**), which was consistent with its mRNA expression (**Fig. S4B**). IHC of CLOCK and
417 BMAL1 corroborated the western blot data (**Fig. S4A**). However, IHC of NR1D1 showed
418 significant localization in the nucleus in PFOA, PFOS, and GenX exposed humanized
419 mice with little localization in the control group (**Fig. 5D**). Further, we performed
420 Western blot analysis of NR1D1, CLOCK, and BMAL1 using cytoplasmic and nuclear

421 fractions, which yielded similar results showing no change in CLOCK and BMAL1 and a
422 significant amount of NR1D1 protein in the nucleus (**Fig. 5E**).

423
424 Due to the strong translocation of NR1D1 into the nucleus and the absence of
425 suppressed BMAL1 expression, we examined whether PFAS directly inhibits NR1D1.
426 To do this, we performed *in silico* ligand docking with each PFAS into the crystalized
427 structure of the DNA-binding domain of NR1D1. We found that PFOA, PFOS, and GenX
428 all docked successfully into the DNA-binding pocket, with delta G values of -7.0, -6.5,
429 and -5.4, respectively (**Fig. 6A–C**). Altogether, our data utilizing humanized mice
430 indicate that PFAS inhibit NR1D1-mediated regulation of circadian rhythm genes (**Fig.**
431 **6D**).

432 **Discussion**

433 *A novel model to identify AOPs involved in PFAS toxicity*

434 PFAS such as PFOA, PFOS, and GenX are activators of PPAR α the primary
435 mechanism by which PFAS induce hepatotoxicity (Conley et al. 2022; He et al. 2022;
436 Pan et al. 2021; Robarts et al. 2022b; Rosen et al. 2010; Wang et al. 2017; Wolf et al.
437 2008). In rodents, PPAR α activation is the first key event (KE) in the development of
438 hepatotoxicity (Corton et al. 2018). However, in humans, PPAR α activation is not
439 thought to be a KE due to lower expression levels of full-length PPAR α compared to
440 rodents (Corton et al. 2018; Palmer et al. 1998) and to a lesser extent differences in
441 affinities between species (Keller et al. 1997; Takacs and Abbott 2007). Because of this,
442 studies in *Ppara*-null rodents and *in vitro* models including primary human hepatocytes,
443 organoids, and cell spheroids have been conducted and to identify important human
444 relevant mechanistic information (Beggs et al. 2016; Reardon et al. 2021; Robarts et al.
445 2022b; Rowan-Carroll et al. 2021; Schlezinger et al. 2021). One issue with *in vitro*
446 models is the lack of cell-cell communication and cross-organ communication that are
447 critical contributors to toxicity mechanisms. In that regard, the humanized-mouse model
448 used in these studies can overcome many of these challenges, because the mice
449 possess human hepatocytes and an intact *in vivo* system, which can potentially reveal
450 more human-relevant AOPs. This was exhibited in which no changes in circadian
451 rhythm were detected in the human spheroid dataset. In addition, PPAR α activation in
452 humanized mouse models was less prominent in human hepatocytes compared to
453 rodent hepatocytes utilizing the agonist fenofibrate (de la Rosa Rodriguez et al. 2018).
454 Our study corroborates this with an induction of rodent PPAR α target gene expression,
455 while no change in the expression of the orthologous human gene.

456 *Cholesterol and bile acid alterations induced by PFAS exposure.*

457 One of the main findings of epidemiological studies was that PFAS (particularly PFOA
458 and PFOS) exposure has a strong correlation with increasing cholesterol levels in
459 serum (Andersen et al. 2021; Blake and Fenton 2020; Frisbee et al. 2010; Rogers et al.
460 2021; Rosato et al. 2022; Steenland et al. 2009). Steenland et al. (2009) found that with
461 increasing PFOA and PFOS concentrations, the odds ratio of having higher levels of
462 cholesterol increased, particularly in LDL/VLDL but not HDL. Another study showed that
463 in children PFOA and PFOS were significantly associated with increases in serum total
464 cholesterol and LDL levels (Frisbee et al. 2010). These data suggest that, in humans,
465 PFAS exposure leads to hypercholesterolemia. The effect of GenX exposure on
466 cholesterol levels is unknown. Our data showing a decrease in total cholesterol after
467 PFOS exposure in humanized mice contradict the epidemiology studies. One possibility
468 behind this discrepancy could be that our model exposure window (28 days) was not
469 adequately long enough to induce hypercholesterolemia. When measuring the specific
470 forms of cholesterol, we found that GenX did significantly induce LDL/VLDL with a slight
471 decrease in HDL, indicating that it could potentially affect cholesterol levels in humans.
472 Interestingly, these cholesterol changes in GenX were accompanied by a decrease of
473 lipid accumulation in the liver. This could be attributed to the increased flux of lipids in
474 the form of LDL/VLDL into the serum. Whereas PFOA had an increase in lipid
475 deposition in the liver with no changes in LDL/VLDL but had a trend in decreased HDL.
476 The flux of lipids out of the liver could explain these steatosis phenotypes.

478
479 We observed a significant increase in serum bile acids following PFOS and GenX
480 treatments. Bile acids are produced from cholesterol by a series of steps, the first of
481 which is catalyzed by the hepatic CYP7A1 enzyme. However, no significant differences
482 in the expression of *CYP7A1* were observed in PFOA, PFOS, and GenX exposed
483 humanized mice. This suggests that changes in serum bile acids are independent of de
484 novo synthesis. We speculate that the increase of bile acids in the serum of GenX and
485 PFOS exposed mice is due to changes in their disposition. It is known that PFAS,
486 including PFOA and PFOS, inhibits the human sodium taurocholate cotransporting
487 polypeptide (NTCP) (Ruggiero et al. 2021; Zhao et al. 2015). NTCP is one of the major
488 bile acid influx transporters located on the basolateral sides of hepatocytes (Watashi et
489 al. 2014). At 10 μ M concentrations, PFOS act as inhibitors of NTCP, displacing bile
490 acids, which in turn increases the serum levels of bile acids (Zhao et al. 2015). The
491 serum concentrations for PFOS in our model was 8.96 μ M, potentially in the NTCP
492 inhibition range. Further studies are needed to determine the inhibitory effects of GenX
493 on NTCP or other bile acid transporters, such as OATs and OATPs. Our data showed
494 no significant increase in serum bile acids in PFOA treated mice. This could be partly
495 due to the large variability in bile acid levels within the treatment group. As most PFAS
496 studies have been on the effects of bile acid transporters *in vitro*, more *in vivo*
497 experiments are needed to clarify the role of bile acid transporters in the deposition of
498 PFAS.

499
500 *Induction of proliferation in response to PFAS exposure.*
501 PFAS induce cell proliferation in rodent livers through PPAR α (Corton et al. 2018;
502 Klaunig et al. 2003). However, because PPAR α RNA and protein is expressed at higher
503 levels in rodents compared to humans and has slightly different ligand binding domains
504 of PPAR α , relevance of PPAR α activation as a mechanism has been questioned
505 (Corton et al. 2014; Thomas et al. 2015; Wolf et al. 2008). Humanized mice treated with
506 fenofibrate, a PPAR α agonist, induced proliferation in only mouse hepatocytes and not
507 human hepatocytes, indicating that proliferation induced by PFAS in humanized mice is
508 PPAR α -independent (Tateno et al. 2015) Previous studies from our group using primary
509 human hepatocytes showed significant induction of the cell cycle gene *CCND1* by
510 PFOA and PFOS (Beggs et al. 2016), and several prometogenic proteins, including Ki67
511 and CDK4 by GenX (Robarts et al. 2022b). The humanized mouse studies corroborated
512 these findings and demonstrated that PFOA, PFOS, and GenX induced proliferation in
513 human hepatocytes *in vivo*. We observed a significant increase in Ki67 and PCNA
514 staining after PFOA and PFOS treatments, with a trend toward an increase following
515 GenX exposure. This was accompanied by the induction of CCND1 protein expression
516 in GenX, PFOA, and PFOS. Taken together, these data, along with previously
517 published primary human hepatocyte exposures, show that PFOA, PFOS, and GenX
518 induce PPAR α independent hepatocyte proliferation at these occupationally relevant
519 concentrations. Intriguingly, an increase in proliferation did not lead to an increase in the
520 liver-weight-to-body-weight ratios of the humanized mice. One explanation could be a
521 concomitant increase in cell death, both apoptosis and possibly necroptosis, after PFAS
522 exposure. Our RNA-Seq data revealed significant activation of p53 in all PFAS exposed
523 mice as compared to the control group, indicating a balance between cell proliferation

524 and cell death. This suggests that PFAS could act as a promoter in hepatocellular
525 carcinomas in hepatocytes possessing loss of function mutations in p53.

526
527 *Implications of changes in NR1D1 activity after PFAS exposure.*

528 One of the most intriguing findings of our studies is the induction of NR1D1, a nuclear
529 receptor involved in the regulation of circadian rhythm, by all three PFAS. In general,
530 light is the signal that starts clock synchronization across organs. The signal from the
531 optic nerve travels to the suprachiasmatic nucleus (SCN) in the hypothalamus, which
532 then communicates with the organs utilizing a variety of cellular and molecular cues,
533 within the endocrine and nervous systems (Mukherji et al. 2019; Tahara and Shibata
534 2016). The orphan nuclear receptor NR1D1 (also known as Rev-Erb α), which functions
535 as a transcriptional suppressor, regulates the intracellular circadian clock
536 (Ramakrishnan and Muscat 2006). During the rest phase or night cycle, the two
537 transcription factors BMAL1 and CLOCK heterodimerize, bind to the E-box promoter,
538 and upregulate a plethora of genes, including proteins involved in the negative feedback
539 loop, such as *PER1/2*, *CRY1/2*, *NR1D1*, and *NR1D2* (Mukherji et al. 2019). During the
540 active phase or light cycle, NR1D1 binds to the E-box promoter of BMAL1,
541 transcriptionally inhibiting BMAL1 production. This in turn decreases *NR1D1* mRNA
542 levels until the night cycle when BMAL1 expression increases due to the loss of
543 NR1D1 (Mukherji et al. 2019). Dysregulation of this feedback loop is known to enhance
544 liver disease progression, making it a critical KE in the AOP of hepatotoxicity (Mukherji
545 et al. 2019; Tahara and Shibata 2016).

546
547 The effects of PFAS on circadian rhythm have never been documented. Our studies
548 indicate that PFOA, PFOS, and GenX could disrupt circadian rhythm through the
549 inhibition of NR1D1. We found an increase in E-box target genes, including a significant
550 induction of *NR1D1* mRNA and protein. However, when measuring BMAL1 levels, there
551 were very few differences between the treatments and control groups, indicating that
552 NR1D1 activity is preferentially inhibited by these PFAS. Studies on determining cellular
553 location, such as IHC and nuclear/cytoplasmic western blots, indicated that NR1D1 is
554 heavily localized in the nucleus, indicating that PFAS do not interfere with nuclear
555 translocation. However, *in silico* modeling suggests that PFOA, PFOS, and GenX all
556 directly inhibit NR1D1 by binding to its DNA-binding domain. Because circadian rhythm
557 regulates multiple processes, including xenobiotic absorption, distribution, metabolism,
558 and excretion, and because its disruption exacerbates liver diseases, it is critical to
559 understand whether PFAS are circadian rhythm disruptors (Baraldo 2008; Tahara and
560 Shibata 2016). Future studies are necessary to investigate the full impact of PFAS on
561 circadian rhythm utilizing human cells and humanized mice.

562
563 The humanized liver model comes with two main caveats. First, there may be a
564 disruption in the cross talk between tissues/cells originating from mice and human
565 hepatocytes. Apart from the hepatocytes, all other non-parenchymal cells and other
566 organs are of mouse origin. The second limitation is that the hepatocytes used for
567 repopulation are all derived from a single human donor, which can lead to individual
568 bias.

569

570 In summary, our studies demonstrate that it is important to study PFAS in human-
571 relevant models. These data indicate that humanized mice are an excellent model to
572 identify human relevant AOPs of toxic exposure.

573

574 **Acknowledgements**

575 The research support for this work was from NIH [grant numbers P20 RR021940-03 &
576 S10 OD021743], NIH NIGMS [grant numbers P30 GM118247 & P30 GM122731], and
577 NIH NIDDK [grant numbers NIH R01 DK0198414 & NIH R56 DK112768]. In addition,
578 we thank Kaberi P Das for her technical support in the mass spectrometry analysis and
579 Dr. Mark J. Strynar for measuring the PFAS in the serum and liver samples.

580 **References**

- 581 Adams PD, Afonine PV, Bunkoczi G, Chen VB, Davis IW, Echols N, et al. 2010. Phenix:
582 A comprehensive python-based system for macromolecular structure solution. *Acta*
583 *Crystallogr D Biol Crystallogr* 66:213-221.
- 584 Akakpo JY, Ramachandran A, Duan L, Schaich MA, Jaeschke MW, Freudenthal BD, et
585 al. 2019. Delayed treatment with 4-methylpyrazole protects against acetaminophen
586 hepatotoxicity in mice by inhibition of c-jun n-terminal kinase. *Toxicol Sci* 170:57-68.
- 587 Andersen ME, Hagenbuch B, Apte U, Corton JC, Fletcher T, Lau C, et al. 2021. Why is
588 elevation of serum cholesterol associated with exposure to perfluoroalkyl substances
589 (pfas) in humans? A workshop report on potential mechanisms. *Toxicology* 459:152845.
- 590 Apte U, Singh S, Zeng G, Cieply B, Virji MA, Wu T, et al. 2009. Beta-catenin activation
591 promotes liver regeneration after acetaminophen-induced injury. *Am J Pathol* 175:1056-
592 1065.
- 593 Azuma H, Paulk N, Ranade A, Dorrell C, Al-Dhalimy M, Ellis E, et al. 2007. Robust
594 expansion of human hepatocytes in *fah^{-/-}rag2^{-/-}il2rg^{-/-}* mice. *Nat Biotechnol* 25:903-
595 910.
- 596 Baraldo M. 2008. The influence of circadian rhythms on the kinetics of drugs in humans.
597 *Expert Opin Drug Metab Toxicol* 4:175-192.
- 598 Beggs KM, McGreal SR, McCarthy A, Gunewardena S, Lampe JN, Lau C, et al. 2016.
599 The role of hepatocyte nuclear factor 4-alpha in perfluorooctanoic acid- and
600 perfluorooctanesulfonic acid-induced hepatocellular dysfunction. *Toxicol Appl*
601 *Pharmacol* 304:18-29.
- 602 Blake BE, Fenton SE. 2020. Early life exposure to per- and polyfluoroalkyl substances
603 (pfas) and latent health outcomes: A review including the placenta as a target tissue
604 and possible driver of peri- and postnatal effects. *Toxicology* 443:152565.
- 605 Brennan NM, Evans AT, Fritz MK, Peak SA, von Holst HE. 2021. Trends in the
606 regulation of per- and polyfluoroalkyl substances (pfas): A scoping review. *Int J Environ*
607 *Res Public Health* 18.
- 608 Chang ET, Adami HO, Boffetta P, Cole P, Starr TB, Mandel JS. 2014. A critical review
609 of perfluorooctanoate and perfluorooctanesulfonate exposure and cancer risk in
610 humans. *Crit Rev Toxicol* 44 Suppl 1:1-81.
- 611 Chappell GA, Thompson CM, Wolf JC, Cullen JM, Klaunig JE, Haws LC. 2020.
612 Assessment of the mode of action underlying the effects of genx in mouse liver and
613 implications for assessing human health risks. *Toxicol Pathol* 48:494-508.
- 614 Conley JM, Lambright CS, Evans N, Medlock-Kakaley E, Hill D, McCord J, et al. 2022.
615 Developmental toxicity of nafion byproduct 2 (nbp2) in the sprague-dawley rat with

- 616 comparisons to hexafluoropropylene oxide-dimer acid (hfpo-da or genx) and
617 perfluorooctane sulfonate (pfos). *Environ Int* 160:107056.
- 618 Corton JC, Cunningham ML, Hummer BT, Lau C, Meek B, Peters JM, et al. 2014. Mode
619 of action framework analysis for receptor-mediated toxicity: The peroxisome proliferator-
620 activated receptor alpha (pparalpha) as a case study. *Crit Rev Toxicol* 44:1-49.
- 621 Corton JC, Peters JM, Klaunig JE. 2018. The pparalpha-dependent rodent liver tumor
622 response is not relevant to humans: Addressing misconceptions. *Arch Toxicol* 92:83-
623 119.
- 624 Cunningham ML, Collins BJ, Hejtmancik MR, Herbert RA, Travlos GS, Vallant MK, et al.
625 2010. Effects of the pparalpha agonist and widely used antihyperlipidemic drug
626 gemfibrozil on hepatic toxicity and lipid metabolism. *PPAR Res* 2010.
- 627 de la Rosa Rodriguez MA, Sugahara G, Hooiveld G, Ishida Y, Tateno C, Kersten S.
628 2018. The whole transcriptome effects of the pparalpha agonist fenofibrate on livers of
629 hepatocyte humanized mice. *BMC Genomics* 19:443.
- 630 Dobin A, Davis CA, Schlesinger F, Drenkow J, Zaleski C, Jha S, et al. 2013. Star:
631 Ultrafast universal rna-seq aligner. *Bioinformatics* 29:15-21.
- 632 Domingo JL, Nadal M. 2019. Human exposure to per- and polyfluoroalkyl substances
633 (pfas) through drinking water: A review of the recent scientific literature. *Environ Res*
634 177:108648.
- 635 Fenton SE, Ducatman A, Boobis A, DeWitt JC, Lau C, Ng C, et al. 2021. Per- and
636 polyfluoroalkyl substance toxicity and human health review: Current state of knowledge
637 and strategies for informing future research. *Environ Toxicol Chem* 40:606-630.
- 638 Foquet L, Schafer C, Minkah NK, Alanine DGW, Flannery EL, Steel RWJ, et al. 2018.
639 *Plasmodium falciparum* liver stage infection and transition to stable blood stage
640 infection in liver-humanized and blood-humanized frgn ko mice enables testing of blood
641 stage inhibitory antibodies (reticulocyte-binding protein homolog 5) in vivo. *Front*
642 *Immunol* 9:524.
- 643 Frisbee SJ, Shankar A, Knox SS, Steenland K, Savitz DA, Fletcher T, et al. 2010.
644 Perfluorooctanoic acid, perfluorooctanesulfonate, and serum lipids in children and
645 adolescents: Results from the c8 health project. *Arch Pediatr Adolesc Med* 164:860-
646 869.
- 647 Fu J, Gao Y, Cui L, Wang T, Liang Y, Qu G, et al. 2016. Occurrence, temporal trends,
648 and half-lives of perfluoroalkyl acids (pfaas) in occupational workers in china. *Sci Rep*
649 6:38039.
- 650 Gebbink WA, van Leeuwen SPJ. 2020. Environmental contamination and human
651 exposure to pfaas near a fluorochemical production plant: Review of historic and current
652 pfoa and genx contamination in the netherlands. *Environ Int* 137:105583.

- 653 Guillette TC, McCord J, Guillette M, Polera ME, Rachels KT, Morgeson C, et al. 2020.
654 Elevated levels of per- and polyfluoroalkyl substances in cape fear river striped bass
655 (*Morone saxatilis*) are associated with biomarkers of altered immune and liver function.
656 *Environ Int* 136:105358.
- 657 Gunewardena S, Huck I, Walesky C, Robarts D, Weinman S, Apte U. 2022. Progressive
658 loss of hepatocyte nuclear factor 4 alpha activity in chronic liver diseases in humans.
659 *Hepatology* 76:372-386.
- 660 Guo H, Sheng N, Guo Y, Wu C, Xie W, Dai J. 2021. Exposure to genx and its novel
661 analogs disrupts fatty acid metabolism in male mice. *Environ Pollut* 291:118202.
- 662 He Y, Lv D, Li C, Liu X, Liu W, Han W. 2022. Human exposure to f-53b in china and the
663 evaluation of its potential toxicity: An overview. *Environ Int* 161:107108.
- 664 Hopkins ZR, Sun M, DeWitt JC, Knappe DRU. 2018. Recently detected drinking water
665 contaminants: Genx and other per- and polyfluoroalkyl ether acids. *Journal - AWWA*
666 110:13-28.
- 667 Keller H, Devchand PR, Perroud M, Wahli W. 1997. Ppar alpha structure-function
668 relationships derived from species-specific differences in responsiveness to
669 hypolipidemic agents. *Biol Chem* 378:651-655.
- 670 Klaunig JE, Babich MA, Baetcke KP, Cook JC, Corton JC, David RM, et al. 2003.
671 Pparalpha agonist-induced rodent tumors: Modes of action and human relevance. *Crit*
672 *Rev Toxicol* 33:655-780.
- 673 Kupersmidt I, Su QJ, Grewal A, Sundaresh S, Halperin I, Flynn J, et al. 2010.
674 Ontology-based meta-analysis of global collections of high-throughput public data.
675 *PLoS One* 5.
- 676 Kurwadkar S, Dane J, Kanel SR, Nadagouda MN, Cawdrey RW, Ambade B, et al. 2022.
677 Per- and polyfluoroalkyl substances in water and wastewater: A critical review of their
678 global occurrence and distribution. *Sci Total Environ* 809:151003.
- 679 Li Y, Fletcher T, Mucs D, Scott K, Lindh CH, Tallving P, et al. 2018. Half-lives of pfos,
680 pfhxs and pfoa after end of exposure to contaminated drinking water. *Occup Environ*
681 *Med* 75:46-51.
- 682 Lindstrom AB, Strynar MJ, Libelo EL. 2011. Polyfluorinated compounds: Past, present,
683 and future. *Environ Sci Technol* 45:7954-7961.
- 684 Livak KJ, Schmittgen TD. 2001. Analysis of relative gene expression data using real-
685 time quantitative pcr and the $2^{-(\Delta\Delta C_t)}$ method. *Methods* 25:402-408.
- 686 Long KR, Lomonosova E, Li Q, Ponzar NL, Villa JA, Touchette E, et al. 2018. Efficacy
687 of hepatitis b virus ribonuclease h inhibitors, a new class of replication antagonists, in
688 frg human liver chimeric mice. *Antiviral Res* 149:41-47.

- 689 Ma J, Tan X, Kwon Y, Delgado ER, Zarnegar A, DeFrances MC, et al. 2022. A novel
690 humanized model of nash and its treatment with meta4, a potent agonist of met. *Cell*
691 *Mol Gastroenterol Hepatol* 13:565-582.
- 692 Moller A, Ahrens L, Surm R, Westerveld J, van der Wielen F, Ebinghaus R, et al. 2010.
693 Distribution and sources of polyfluoroalkyl substances (pfas) in the river rhine
694 watershed. *Environ Pollut* 158:3243-3250.
- 695 Morris GM, Huey R, Lindstrom W, Sanner MF, Belew RK, Goodsell DS, et al. 2009.
696 Autodock4 and autodocktools4: Automated docking with selective receptor flexibility. *J*
697 *Comput Chem* 30:2785-2791.
- 698 Mukherjee R, Jow L, Noonan D, McDonnell DP. 1994. Human and rat peroxisome
699 proliferator activated receptors (ppars) demonstrate similar tissue distribution but
700 different responsiveness to ppar activators. *J Steroid Biochem Mol Biol* 51:157-166.
- 701 Mukherji A, Bailey SM, Staels B, Baumert TF. 2019. The circadian clock and liver
702 function in health and disease. *J Hepatol* 71:200-211.
- 703 Olsen GW, Burris JM, Ehresman DJ, Froehlich JW, Seacat AM, Butenhoff JL, et al.
704 2007. Half-life of serum elimination of
705 perfluorooctanesulfonate, perfluorohexanesulfonate, and perfluorooctanoate in retired
706 fluorochemical production workers. *Environ Health Perspect* 115:1298-1305.
- 707 Palmer CN, Hsu MH, Griffin KJ, Raucy JL, Johnson EF. 1998. Peroxisome proliferator
708 activated receptor- α expression in human liver. *Mol Pharmacol* 53:14-22.
- 709 Pan Z, Miao W, Wang C, Tu W, Jin C, Jin Y. 2021. 6:2 cl-pfesa has the potential to
710 cause liver damage and induce lipid metabolism disorders in female mice through the
711 action of ppar- γ . *Environ Pollut* 287:117329.
- 712 Rahman MF, Peldszus S, Anderson WB. 2014. Behaviour and fate of perfluoroalkyl and
713 polyfluoroalkyl substances (pfass) in drinking water treatment: A review. *Water Res*
714 50:318-340.
- 715 Ramakrishnan SN, Muscat GE. 2006. The orphan rev-erb nuclear receptors: A link
716 between metabolism, circadian rhythm and inflammation? *Nucl Recept Signal* 4:e009.
- 717 Reardon AJF, Rowan-Carroll A, Ferguson SS, Leingartner K, Gagne R, Kuo B, et al.
718 2021. Potency ranking of per- and polyfluoroalkyl substances using high-throughput
719 transcriptomic analysis of human liver spheroids. *Toxicol Sci* 184:154-169.
- 720 Reiner JL, Nakayama SF, Delinsky AD, Stanko JP, Fenton SE, Lindstrom AB, et al.
721 2009. Analysis of pfoa in dosed cd1 mice. Part 1. Methods development for the analysis
722 of tissues and fluids from pregnant and lactating mice and their pups. *Reprod Toxicol*
723 27:360-364.

- 724 Robarts DR, McGreal SR, Umbaugh DS, Parkes WS, Kotulkar M, Abernathy S, et al.
725 2022a. Regulation of liver regeneration by hepatocyte o-glcncacylation in mice. *Cell Mol*
726 *Gastroenterol Hepatol* 13:1510-1529.
- 727 Robarts DR, Venneman KK, Gunewardena S, Apte U. 2022b. Genx induces
728 fibroinflammatory gene expression in primary human hepatocytes. *Toxicology*
729 477:153259.
- 730 Rogers RD, Reh CM, Breysse P. 2021. Advancing per- and polyfluoroalkyl substances
731 (pfas) research: An overview of atsd and nceh activities and recommendations. *J Expo*
732 *Sci Environ Epidemiol*.
- 733 Rosato I, Zare Jeddi M, Ledda C, Gallo E, Fletcher T, Pitter G, et al. 2022. How to
734 investigate human health effects related to exposure to mixtures of per- and
735 polyfluoroalkyl substances: A systematic review of statistical methods. *Environ Res*
736 205:112565.
- 737 Rosen MB, Schmid JR, Corton JC, Zehr RD, Das KP, Abbott BD, et al. 2010. Gene
738 expression profiling in wild-type and pparalpha-null mice exposed to perfluorooctane
739 sulfonate reveals pparalpha-independent effects. *PPAR Res* 2010.
- 740 Rosen MB, Das KP, Rooney J, Abbott B, Lau C, Corton JC. 2017. Pparalpha-
741 independent transcriptional targets of perfluoroalkyl acids revealed by transcript
742 profiling. *Toxicology* 387:95-107.
- 743 Rowan-Carroll A, Reardon A, Leingartner K, Gagne R, Williams A, Meier MJ, et al.
744 2021. High-throughput transcriptomic analysis of human primary hepatocyte spheroids
745 exposed to per- and polyfluoroalkyl substances (pfas) as a platform for relative potency
746 characterization. *Toxicol Sci*.
- 747 Ruggiero MJ, Miller H, Idowu JY, Zitzow JD, Chang SC, Hagenbuch B. 2021.
748 Perfluoroalkyl carboxylic acids interact with the human bile acid transporter ntcp. *Livers*
749 1:221-229.
- 750 Schlezinger JJ, Hyotylainen T, Sinioja T, Boston C, Puckett H, Oliver J, et al. 2021.
751 Perfluorooctanoic acid induces liver and serum dyslipidemia in humanized pparalpha
752 mice fed an american diet. *Toxicol Appl Pharmacol* 426:115644.
- 753 Sen P, Qadri S, Luukkonen PK, Ragnarsdottir O, McGlinchey A, Jantti S, et al. 2022.
754 Exposure to environmental contaminants is associated with altered hepatic lipid
755 metabolism in non-alcoholic fatty liver disease. *J Hepatol* 76:283-293.
- 756 Sierk ML, Zhao Q, Rastinejad F. 2001. DNA deformability as a recognition feature in the
757 reverb response element. *Biochemistry* 40:12833-12843.
- 758 Steenland K, Tinker S, Frisbee S, Ducatman A, Vaccarino V. 2009. Association of
759 perfluorooctanoic acid and perfluorooctane sulfonate with serum lipids among adults
760 living near a chemical plant. *Am J Epidemiol* 170:1268-1278.

- 761 Stone D, Long KR, Loprieno MA, De Silva Felixge HS, Kenkel EJ, Liley RM, et al.
762 2021. Crispr-cas9 gene editing of hepatitis b virus in chronically infected humanized
763 mice. *Mol Ther Methods Clin Dev* 20:258-275.
- 764 Sunderland EM, Hu XC, Dassuncao C, Tokranov AK, Wagner CC, Allen JG. 2019. A
765 review of the pathways of human exposure to poly- and perfluoroalkyl substances
766 (pfass) and present understanding of health effects. *J Expo Sci Environ Epidemiol*
767 29:131-147.
- 768 Tahara Y, Shibata S. 2016. Circadian rhythms of liver physiology and disease:
769 Experimental and clinical evidence. *Nat Rev Gastroenterol Hepatol* 13:217-226.
- 770 Takacs ML, Abbott BD. 2007. Activation of mouse and human peroxisome proliferator-
771 activated receptors (alpha, beta/delta, gamma) by perfluorooctanoic acid and
772 perfluorooctane sulfonate. *Toxicol Sci* 95:108-117.
- 773 Tateno C, Yamamoto T, Utoh R, Yamasaki C, Ishida Y, Myoken Y, et al. 2015. Chimeric
774 mice with hepatocyte-humanized liver as an appropriate model to study human
775 peroxisome proliferator-activated receptor-alpha. *Toxicol Pathol* 43:233-248.
- 776 Thomas M, Bayha C, Klein K, Muller S, Weiss TS, Schwab M, et al. 2015. The
777 truncated splice variant of peroxisome proliferator-activated receptor alpha, pparalpha-
778 tr, autonomously regulates proliferative and pro-inflammatory genes. *BMC Cancer*
779 15:488.
- 780 Trott O, Olson AJ. 2010. Autodock vina: Improving the speed and accuracy of docking
781 with a new scoring function, efficient optimization, and multithreading. *J Comput Chem*
782 31:455-461.
- 783 Tyagi RK, Tandel N, Deshpande R, Engelman RW, Patel SD, Tyagi P. 2018.
784 Humanized mice are instrumental to the study of plasmodium falciparum infection. *Front*
785 *Immunol* 9:2550.
- 786 Umbaugh DS, Soder RP, Nguyen NT, Adelusi O, Robarts DR, Woolbright B, et al. 2022.
787 Human wharton's jelly-derived mesenchymal stem cells prevent acetaminophen-
788 induced liver injury in a mouse model unlike human dermal fibroblasts. *Archives of*
789 *Toxicology*.
- 790 Walesky C, Gunewardena S, Terwilliger EF, Edwards G, Borude P, Apte U. 2013.
791 Hepatocyte-specific deletion of hepatocyte nuclear factor-4alpha in adult mice results in
792 increased hepatocyte proliferation. *Am J Physiol Gastrointest Liver Physiol* 304:G26-37.
- 793 Wang J, Wang X, Sheng N, Zhou X, Cui R, Zhang H, et al. 2017. Rna-sequencing
794 analysis reveals the hepatotoxic mechanism of perfluoroalkyl alternatives, hfpo2 and
795 hfpo4, following exposure in mice. *J Appl Toxicol* 37:436-444.

- 796 Wang S, Wang X, Tan Z, Su Y, Liu J, Chang M, et al. 2019. Human esc-derived
797 expandable hepatic organoids enable therapeutic liver repopulation and
798 pathophysiological modeling of alcoholic liver injury. *Cell Res* 29:1009-1026.
- 799 Watashi K, Urban S, Li W, Wakita T. 2014. Ntcp and beyond: Opening the door to
800 unveil hepatitis b virus entry. *Int J Mol Sci* 15:2892-2905.
- 801 Wolf CJ, Takacs ML, Schmid JE, Lau C, Abbott BD. 2008. Activation of mouse and
802 human peroxisome proliferator-activated receptor alpha by perfluoroalkyl acids of
803 different functional groups and chain lengths. *Toxicol Sci* 106:162-171.
- 804 Xu Y, Fletcher T, Pineda D, Lindh CH, Nilsson C, Glynn A, et al. 2020. Serum half-lives
805 for short- and long-chain perfluoroalkyl acids after ceasing exposure from drinking water
806 contaminated by firefighting foam. *Environ Health Perspect* 128:77004.
- 807 Zhao W, Zitzow JD, Ehresman DJ, Chang SC, Butenhoff JL, Forster J, et al. 2015.
808 Na⁺/taurocholate cotransporting polypeptide and apical sodium-dependent bile acid
809 transporter are involved in the disposition of perfluoroalkyl sulfonates in humans and
810 rats. *Toxicol Sci* 146:363-373.
811

812 **Tables**

813 *Table 1. Top 20 |fold change| of DEGs that are significantly altered in livers from PFOA,*
 814 *PFOS, and GenX exposed humanized mice.*

815

PFOA			PFOS			GenX		
Gene Symbol	Fold Change	P-Value	Gene Symbol	Fold Change	P-Value	Gene Symbol	Fold Change	P-Value
<i>KRT23</i>	-10.09	2.07E-02	<i>HSPA6</i>	-12.62	4.59E-02	<i>KIF18A</i>	-23.51	1.30E-04
<i>NRN1</i>	-5.93	5.50E-03	<i>GRIP2</i>	-9.29	3.30E-03	<i>MRC2</i>	-10.84	3.64E-03
<i>RGS2</i>	-5.42	5.00E-04	<i>KRT23</i>	-7.52	4.13E-02	<i>PLXNA4</i>	-10.44	6.60E-03
<i>MRC2</i>	-4.93	3.12E-02	<i>ECEL1</i>	7.5	8.90E-03	<i>SLITRK3</i>	-8.38	1.51E-01
<i>UCP2</i>	-4.67	1.52E-02	<i>RASGRP2</i>	-7.3	2.59E-02	<i>ADAMTS1</i>	-8.07	7.62E-04
<i>GNG4</i>	4.15	1.44E-02	<i>SAA1</i>	-5.43	4.23E-05	<i>ESCO2</i>	-7.77	8.96E-05
<i>KIF18A</i>	-4.03	5.70E-03	<i>FRMD3</i>	-4.96	1.03E-02	<i>SIK1B</i>	-7.43	3.00E-02
<i>NEIL3</i>	-3.94	2.54E-02	<i>NRN1</i>	-4.9	1.26E-02	<i>NRN1</i>	-7.00	4.03E-03
<i>CEP55</i>	-3.83	5.50E-03	<i>MRC2</i>	-4.87	3.42E-02	<i>ECEL1</i>	6.82	1.29E-02
<i>SDK1</i>	3.48	9.00E-04	<i>PRODH</i>	4.4	3.50E-03	<i>GFI1</i>	-6.81	4.37E-04
<i>KIF14</i>	-3.31	7.00E-03	<i>LRRC66</i>	-3.7	3.17E-02	<i>NEIL3</i>	-6.42	6.80E-03
<i>PIF1</i>	-3.19	1.23E-02	<i>MSI1</i>	-3.54	2.84E-02	<i>E2F2</i>	-6.35	2.03E-06
<i>PBK</i>	-2.98	7.70E-03	<i>GFI1</i>	-3.36	1.79E-02	<i>VCAN</i>	5.27	1.44E-04
<i>NUF2</i>	-2.9	1.15E-02	<i>COX7A1</i>	3.34	3.59E-02	<i>NEK2</i>	-5.25	4.75E-06
<i>LAMP3</i>	2.88	1.24E-02	<i>NLRP14</i>	3.34	1.60E-03	<i>SAA1</i>	-5.24	6.14E-05
<i>NEK2</i>	-2.88	1.10E-03	<i>GPR88</i>	-3.29	4.07E-02	<i>NUF2</i>	-5.18	4.75E-04
<i>C17orf67</i>	-2.85	1.60E-03	<i>SIK1B</i>	-3.26	2.75E-02	<i>PRODH</i>	4.99	1.49E-03
<i>CDKN1C</i>	2.76	2.12E-02	<i>ADAMTSL2</i>	-3.26	3.82E-02	<i>PLA2G2A</i>	-4.96	4.21E-04
<i>CDKN3</i>	-2.74	4.80E-03	<i>CEP55</i>	-3.09	1.87E-02	<i>FKBP1B</i>	-4.84	1.85E-02
<i>EHF</i>	-2.72	3.83E-02	<i>KIF18A</i>	-3.06	2.41E-02	<i>RGS2</i>	-4.83	1.43E-03

816

817 *Table 2. Common upregulated DEGs between PFOS, PFOA, and GenX exposed mice.*
818

Gene Symbol	PFOA		PFOS		GenX	
	Fold Change	P-Value	Fold Change	P-Value	Fold Change	P-Value
<i>C19orf71</i>	1.53	2.14E-02	1.51	2.57E-02	1.67	5.31E-03
<i>COL6A2</i>	1.68	1.85E-02	2.04	1.24E-03	4.02	2.62E-10
<i>LAMC3</i>	2.62	6.38E-03	2.08	4.36E-02	2.31	2.03E-02
<i>MT1E</i>	2.01	1.34E-02	1.88	2.60E-02	2.20	5.34E-03
<i>MT1F</i>	2.57	2.78E-02	2.62	2.49E-02	3.19	6.97E-03
<i>MT1G</i>	2.47	4.97E-03	2.26	1.12E-02	2.67	2.28E-03
<i>MT1H</i>	2.25	1.42E-02	1.96	4.15E-02	2.17	1.94E-02
<i>MT1M</i>	2.45	3.05E-02	2.52	2.55E-02	3.16	5.53E-03
<i>MT1X</i>	2.52	3.90E-03	2.31	8.99E-03	2.85	1.05E-03
<i>MT2A</i>	1.93	2.31E-02	1.95	2.13E-02	2.24	5.43E-03
<i>MYO16</i>	1.51	2.20E-04	1.53	1.94E-04	1.65	9.36E-06
<i>SPTBN4</i>	2.30	6.37E-03	2.55	2.27E-03	2.47	3.25E-03

819

820 *Table 3. Common downregulated DEGs between PFOS, PFOA, and GenX exposed*
 821 *mice.*
 822

Gene Symbol	PFOA		PFOS		GenX	
	Fold Change	P-Value	Fold Change	P-Value	Fold Change	P-Value
<i>ADAM19</i>	-1.77	2.38E-02	-1.84	1.70E-02	-2.58	3.02E-04
<i>ANLN</i>	-2.20	2.11E-03	-1.73	3.18E-02	-3.66	1.59E-06
<i>BCL2L14</i>	-2.44	3.66E-02	-2.78	2.10E-02	-2.40	4.46E-02
<i>BIRC5</i>	-1.76	2.00E-02	-1.92	7.80E-03	-3.17	6.14E-06
<i>CCNA2</i>	-1.86	6.64E-03	-1.66	2.69E-02	-2.28	4.33E-04
<i>CCNB1</i>	-1.92	5.00E-03	-1.62	3.83E-02	-3.17	2.59E-06
<i>CDC20</i>	-2.65	1.90E-03	-1.92	3.72E-02	-4.06	1.51E-05
<i>CENPE</i>	-2.63	1.65E-03	-2.14	1.25E-02	-2.19	1.07E-02
<i>CYP27B1</i>	-2.00	1.51E-02	-1.76	4.71E-02	-2.51	2.37E-03
<i>CYP3A7</i>	-1.82	1.94E-02	-1.84	1.75E-02	-2.26	1.59E-03
<i>DLGAP5</i>	-1.93	2.60E-02	-1.87	3.59E-02	-3.07	4.99E-04
<i>HSPA5</i>	-1.54	1.57E-04	-1.60	3.70E-05	-1.88	3.20E-08
<i>JCAD</i>	-2.23	3.64E-02	-2.21	4.19E-02	-2.18	4.57E-02
<i>KIF18A</i>	-4.03	5.70E-03	-3.06	2.41E-02	-23.51	1.30E-04
<i>KIF20A</i>	-1.92	3.20E-03	-1.69	1.81E-02	-3.11	1.45E-06
<i>KPNA2</i>	-1.86	1.22E-05	-1.55	2.23E-03	-2.34	4.77E-09
<i>MRC2</i>	-4.93	3.12E-02	-4.87	3.42E-02	-10.84	3.64E-03
<i>NDC80</i>	-1.86	8.72E-03	-1.99	4.82E-03	-2.49	3.14E-04
<i>NEK2</i>	-2.88	1.06E-03	-2.01	2.69E-02	-5.25	4.75E-06
<i>NRN1</i>	-5.93	5.46E-03	-4.90	1.26E-02	-7.00	4.03E-03
<i>RDH12</i>	-2.28	1.74E-02	-2.15	2.81E-02	-2.21	2.32E-02
<i>SLC7A10</i>	-2.10	6.75E-03	-2.74	3.66E-04	-2.99	1.25E-04
<i>TIGAR</i>	-2.29	2.56E-03	-1.89	2.06E-02	-2.24	4.01E-03

823

824 **Figure Legends**

825 **Figure 1. Establishing an *in vivo* human-relevant model to study PFAS.**

826 (A) Scheme of the experimental design. (B) Photomicrographs of IHC for FAH in livers
827 of all treatment groups at both 40x and 100x magnifications, where FAH positive
828 hepatocytes indicate human origin. The small box corresponds to the 200x
829 magnification image. Arrowheads are examples of mouse derived hepatocytes. Mass
830 spectrometry analysis of (C) serum and (D) liver PFAS concentrations. The bar
831 represents the mean \pm SEM. (E) Liver H&E photomicrographs of all treatment groups at
832 200x magnification. The small box corresponds to the 400x magnification image.

833
834 **Figure 2. Serum profiles and hepatic lipid deposition of humanized mice exposed
835 to PFAS.**

836 (A) Liver weight-to-body weight percentage in all treatment groups. Measurements of
837 (B) ALT, (C) Glucose, (D) Triglycerides, (E) Free Fatty Acids, (F) Total Cholesterol, (G)
838 LDL and VLDL, (H) HDL, and (I) bile acids in the serum of all treatment groups. Bar
839 graphs represent the mean \pm SEM, where * $p < 0.05$, ** $p < 0.01$ and *** $p < 0.001$. (J)
840 Photomicrographs of Oil Red O staining in the livers of all treatment groups to indicate
841 lipid deposition.

842
843 **Figure 3. PFAS induced significant proliferation in Humanized Mice after 28 day
844 exposure.**

845 (A) Photomicrographs (200X) of Ki67 and PCNA. The small box corresponds to the
846 400x magnification image. IHC in the livers of all treatment groups with respective
847 quantification at 200x magnifications of positive (B) cell number and (C) cell percentage.
848 (D) Gene expression analysis using qPCR on the proliferative genes Cyclin D1
849 (*CCND1*). Data were normalized to 18s and then to the control group. Bar graphs
850 represent the mean \pm SEM. (E) Western blot analysis of whole liver lysates for the
851 proliferative mitogens cyclin D1, phosphorylated RB, CDK4, and CDK1 with β -actin as a
852 loading control.

853
854 **Figure 4. PFAS induces significant transcriptome alterations and upstream
855 regulators.**

856 Volcano plots of the DEGs from the (A) PFOA, (B) PFOS, and (C) GenX treated
857 humanized mice, where red and blue dots represent significantly upregulated and
858 downregulated genes, respectively. The blue dashed lines represent a Fold Change of
859 1.5, and the red dashed line represents a p-value of 0.05. Venn diagrams of DEGs of
860 (D) upregulated and (E) downregulated genes, with shades of red representing the
861 number of DEGs in each segment of the diagram. Dot plot of the IPA upstream analysis
862 for (F) PFOA, (G) PFOS, and (H) GenX. The color represents the $\log_2(p\text{-value})$, the size
863 of the dot represents the number of DEGs in the pathway, the z-score represents the
864 activation status (negative = inhibition and positive = activation), and the red dashed line
865 represents a z-score of 0.

866
867 **Figure 5. NR1D1 was significantly induced in all PFAS treatment groups.**

868 (A) qPCR analysis of livers from PFAS treatment groups of E-box regulated genes,
869 including *NR1D1*, *CRY2*, *PER2*, and *PER1*. Samples were first normalized to the

870 housekeeping gene 18s and then to the control group. (B) Western blot analysis of
871 NR1D1 and the regulators BMAL1 and CLOCK. GAPDH was used as a loading control.
872 (C) Densitometric analysis of the western blots, where the densitometry of each band
873 was normalized to GAPDH. (D) Photomicrographs of liver IHC of NR1D1 from PFAS
874 treated mice at 200x resolution. The small box corresponds to the 400x magnification
875 image. (E) Western blot analysis of nuclear and cytoplasmic fractionation from control
876 and PFAS treated livers of NR1D1, CLOCK, and BMAL1. Histone 3 and α -tubulin were
877 used as loading controls for the nuclear and cytoplasmic fractions, respectively. (F)
878 Densitometry of the fractionated western blots. All bar graphs represent the mean \pm
879 SEM. * $p < 0.05$, ** $p < 0.01$ and *** $p < 0.001$

880
881 **Figure 6. PFAS act as an NR1D1 antagonist by binding to the DNA binding**
882 **domain.**

883 Docking of (B) PFOA, (C) PFOS, and (D) GenX into the crystal structure of NR1D1, with
884 corresponding delta G values and predicted protein-compound interactions. (E)
885 Mechanism of action of PFAS through NR1D1, causing dysregulation of the circadian
886 rhythm E-box pathway.

887
888 **Supplementary Figure 1. PFAS caused an induction of PPAR α target genes**
889 **expression in mouse hepatocytes and not in humans.**
890 qPCR of *Cpt1a/CPT1A* and *Hmgcs2/HMGCS2* using rodent and human specific primers
891 in (A) PFOA, (B) PFOS, and (C) GenX treated humanized mice. Fold changes are
892 relative to the untreated group. Gene expressions were normalized to the respective
893 species housekeeping gene (*Gapdh/GAPDH*). Connecting lines represent expression of
894 mouse and human genes derived from the same liver with bars representing the
895 average fold change.

896
897 **Supplementary Figure 2. Global changes of RNA-Seq of humanized mice treated**
898 **with PFOA, PFOS, GenX.**

899 (A) Connecting bar plot of the expression level of ligand-binding nuclear receptors in
900 livers of human and control humanized mice, where the y-axis is the gene, and the x-
901 axis is the normalized DESeq2 normalized counts. Expression levels were ranked from
902 highest to lowest, with the black line linking the gene of each species. Heatmap of (B)
903 global gene expression, (C) cytochrome P450 metabolizing enzymes, and (D) phase 2
904 enzymes. Blue and orange represent negative and positive fold changes, respectively.

905
906 **Supplementary Figure 3. RNA-Sequencing of PFOA and PFOS treated humanized**
907 **mice is significantly correlated with human hepatic spheroids exposed to PFOS**
908 **and PFOA for 14 days.**

909 (A) Heatmap of $-\log(p\text{-values})$ from BSCE comparing the DEGs from exposed human
910 hepatic spheroids and the treated humanized mice. Blue and orange represent negative
911 and positive correlations, respectively, and no assigned p-value is represented by gray.
912 Column colors represent the compound (PFOA or PFOS) the spheroids were exposed
913 to, the exposure time (1, 4, 10, 14 days), and the concentration of the compound (0.02,
914 0.2, 1, 2, 10, 20, 50 μM). Each number in the cells of the heatmap represents the
915 significant $-\log(p\text{-value})$ s with no number indicating no significance. Line graphs of each

916 -log(p-value) for (B) PFOS and (C) PFOA exposed human hepatic spheroids. Where
917 color and shape indicate the length of spheroid exposure, the y-axis represents the -
918 log(p-value) and the x-axis represents the concentration (μM) exposed to the spheroids.

919

920 **Supplementary Figure 4. PFAS caused no change in BMAL1 and CLOCK nuclear**
921 **localization.**

922 (A) Photomicrographs of liver IHC of BMAL1 and CLOCK for control and PFAS treated
923 humanized mice at 200x. The small box corresponds to the 400x magnification image.

924 (B) qPCR of *ARNTL* (BMAL1 gene), where samples were first normalized to the 18s
925 housekeeping gene and then to the control group. Bars represent mean \pm SEM.

926

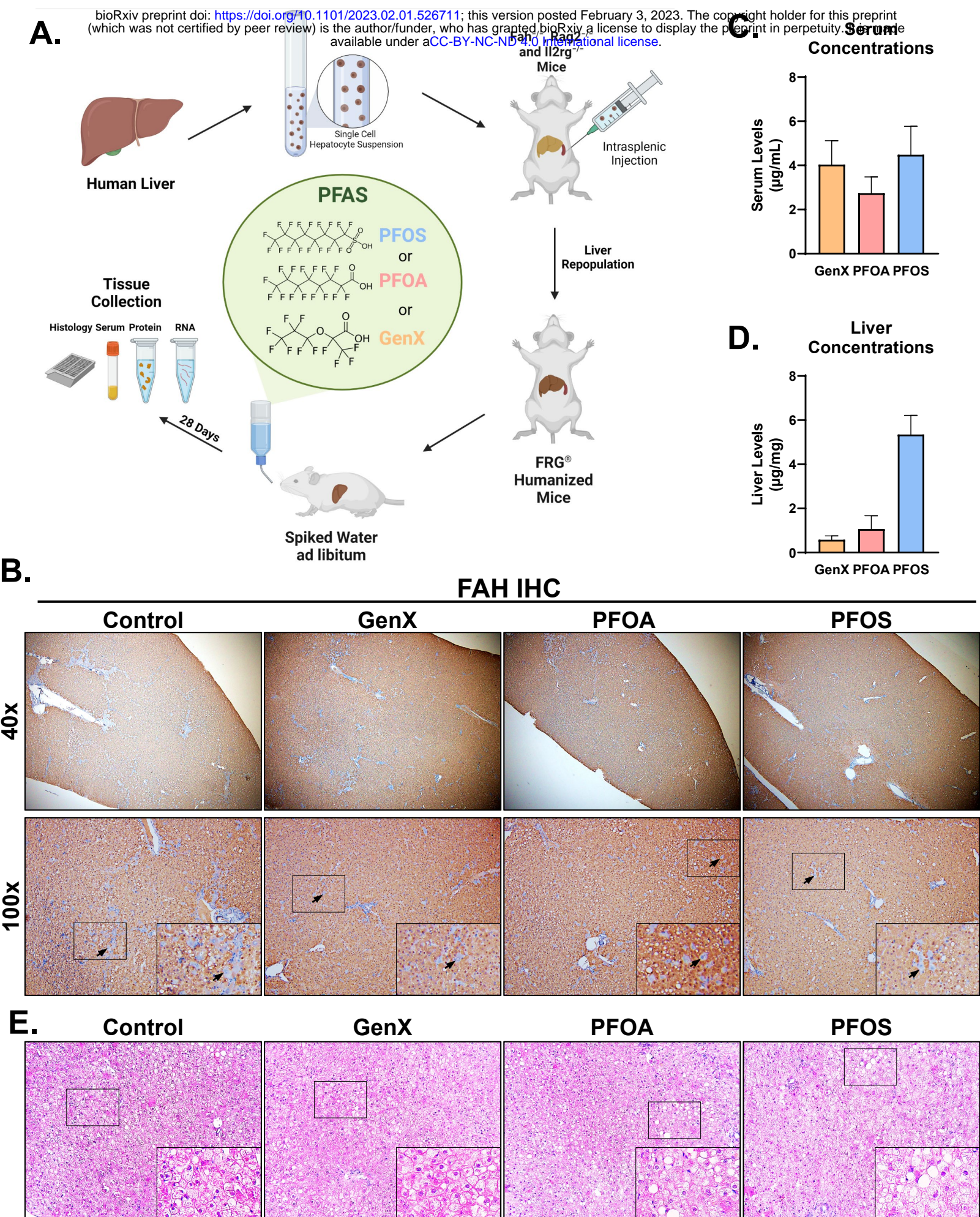


Figure 1

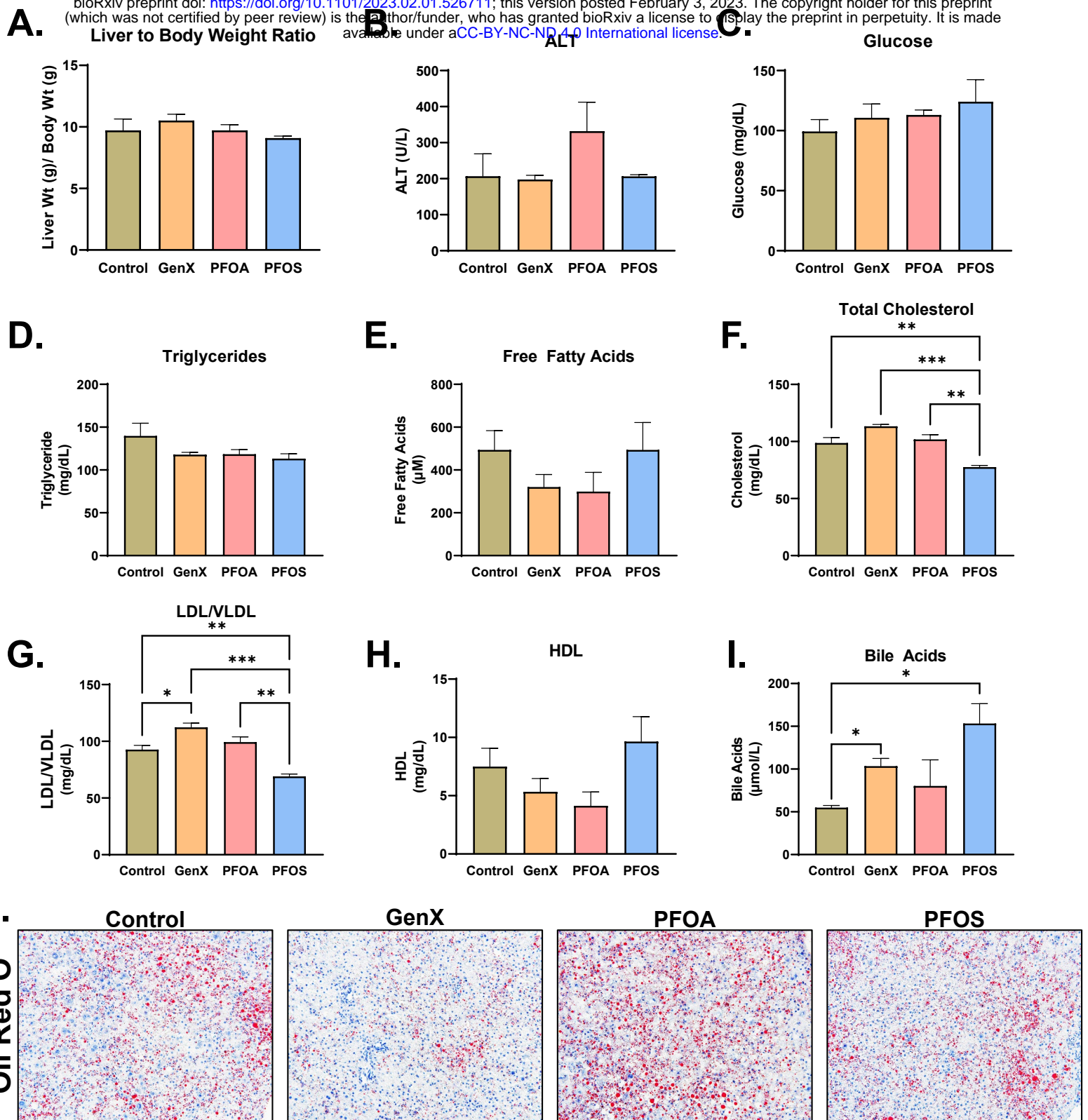


Figure 2

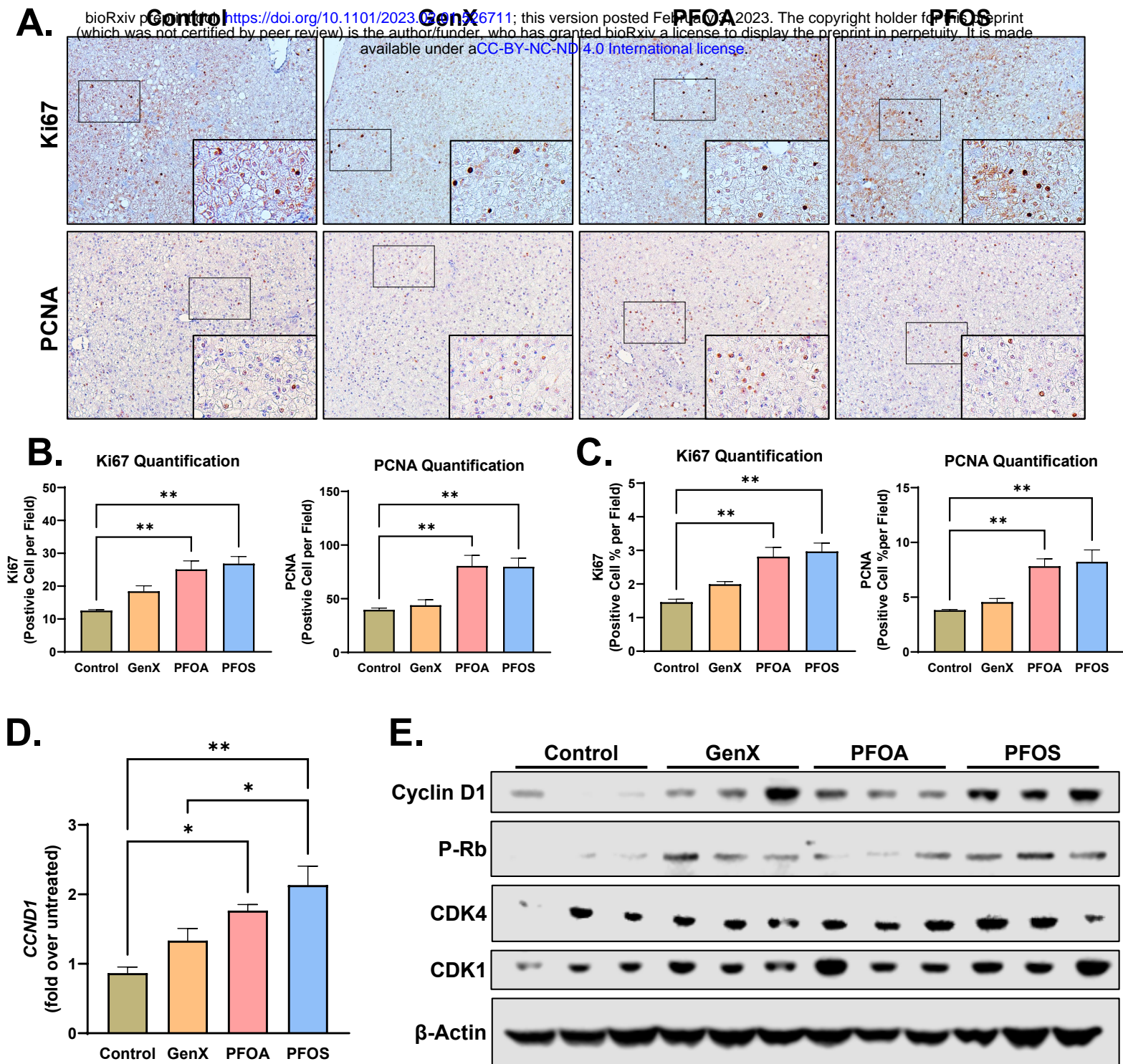


Figure 3

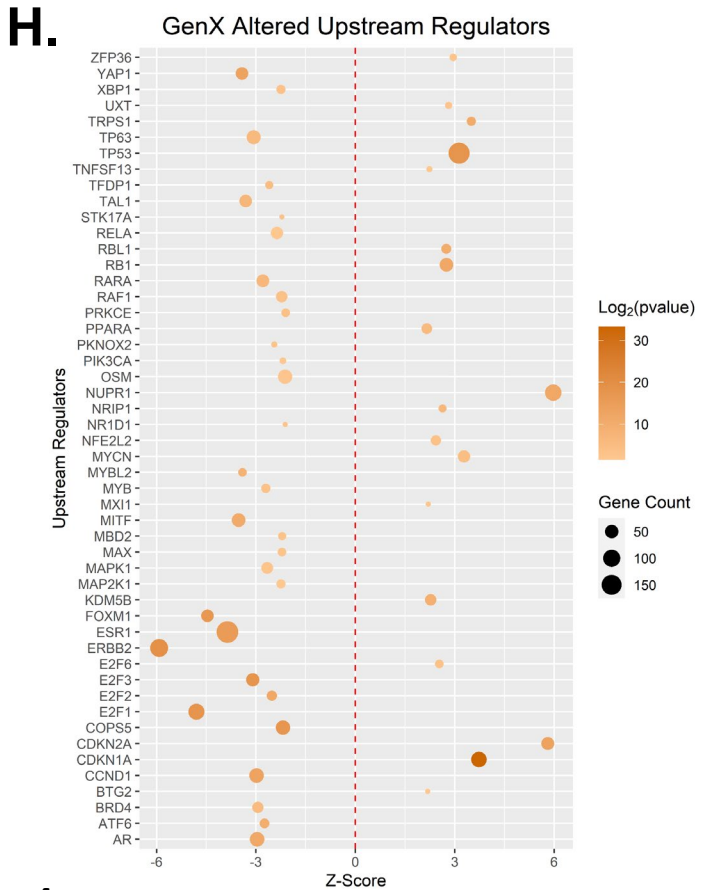
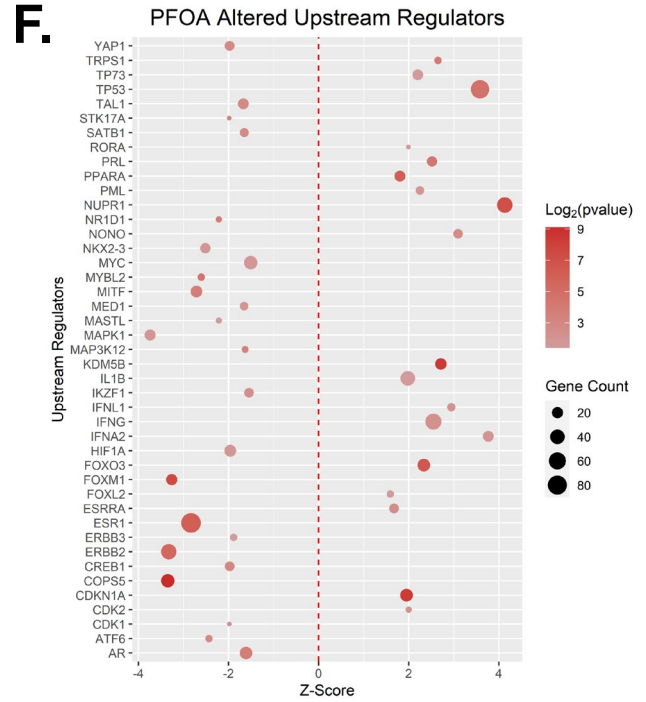
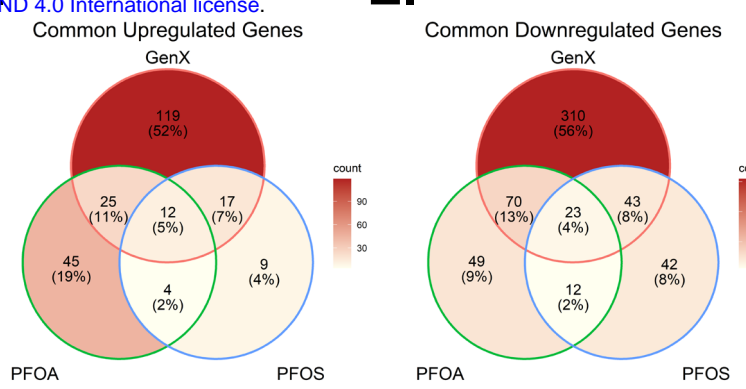
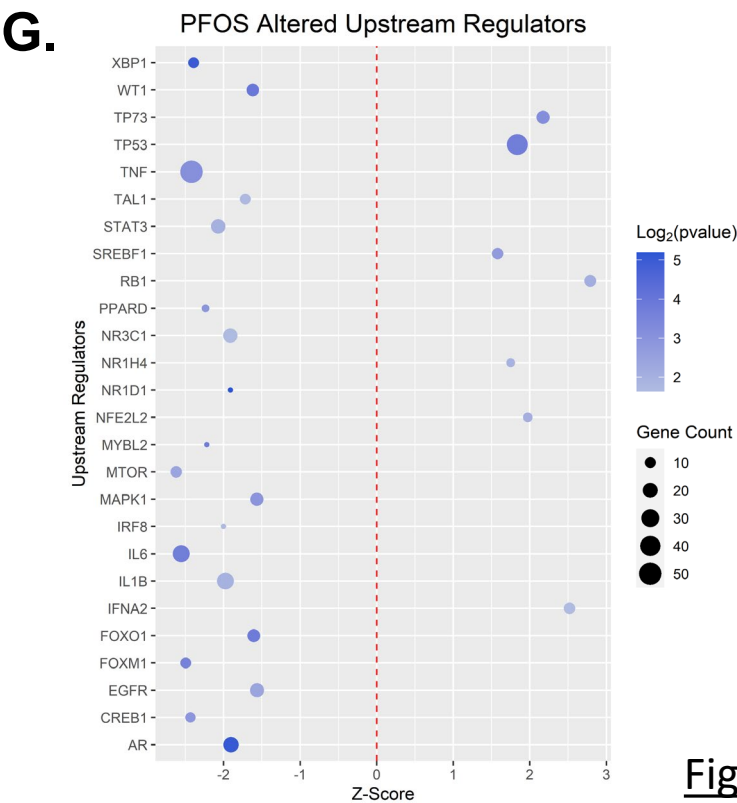
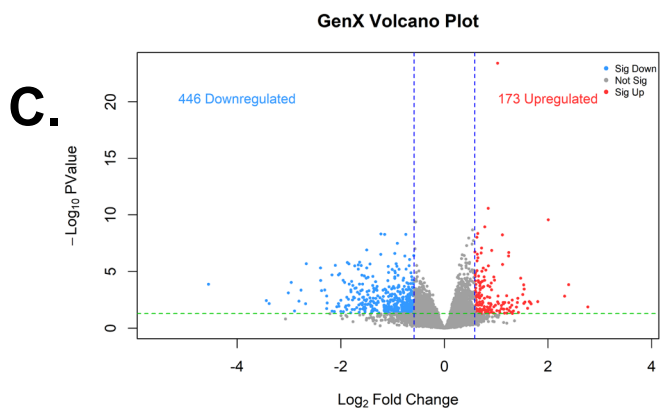
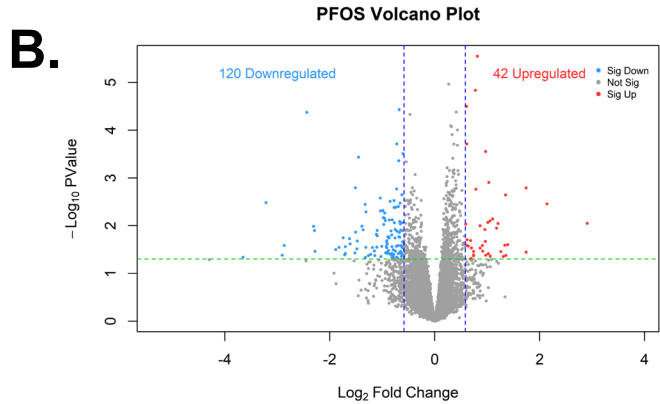
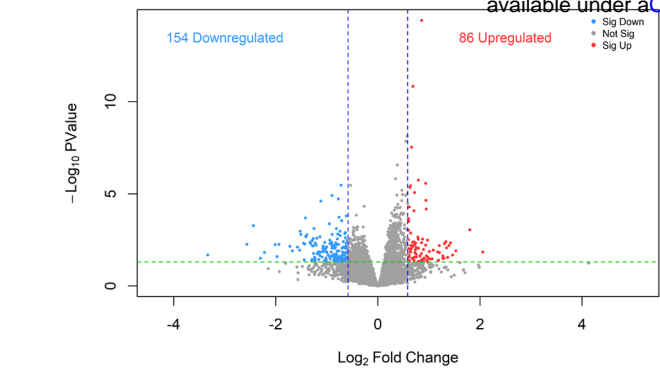


Figure 4

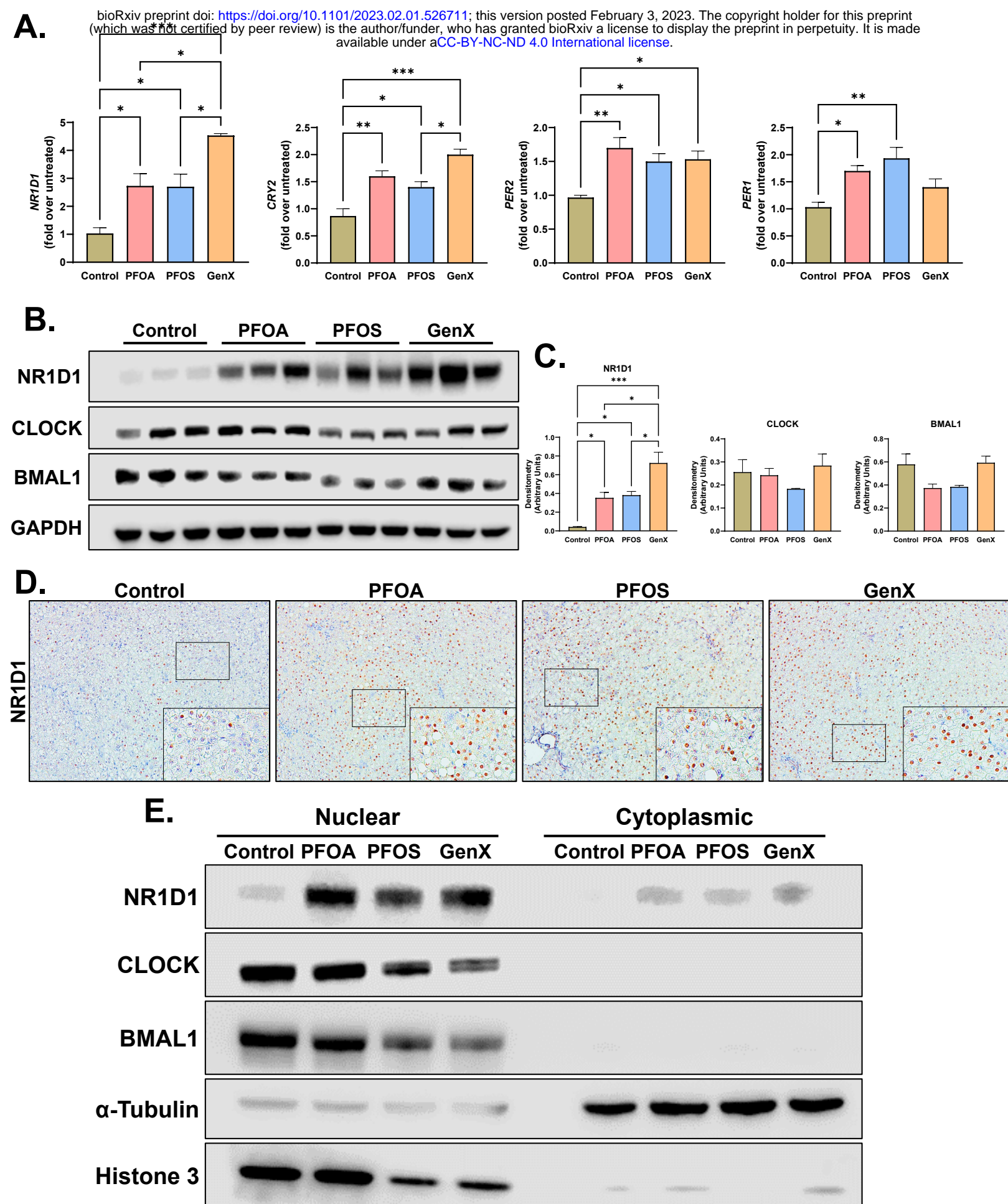


Figure 5

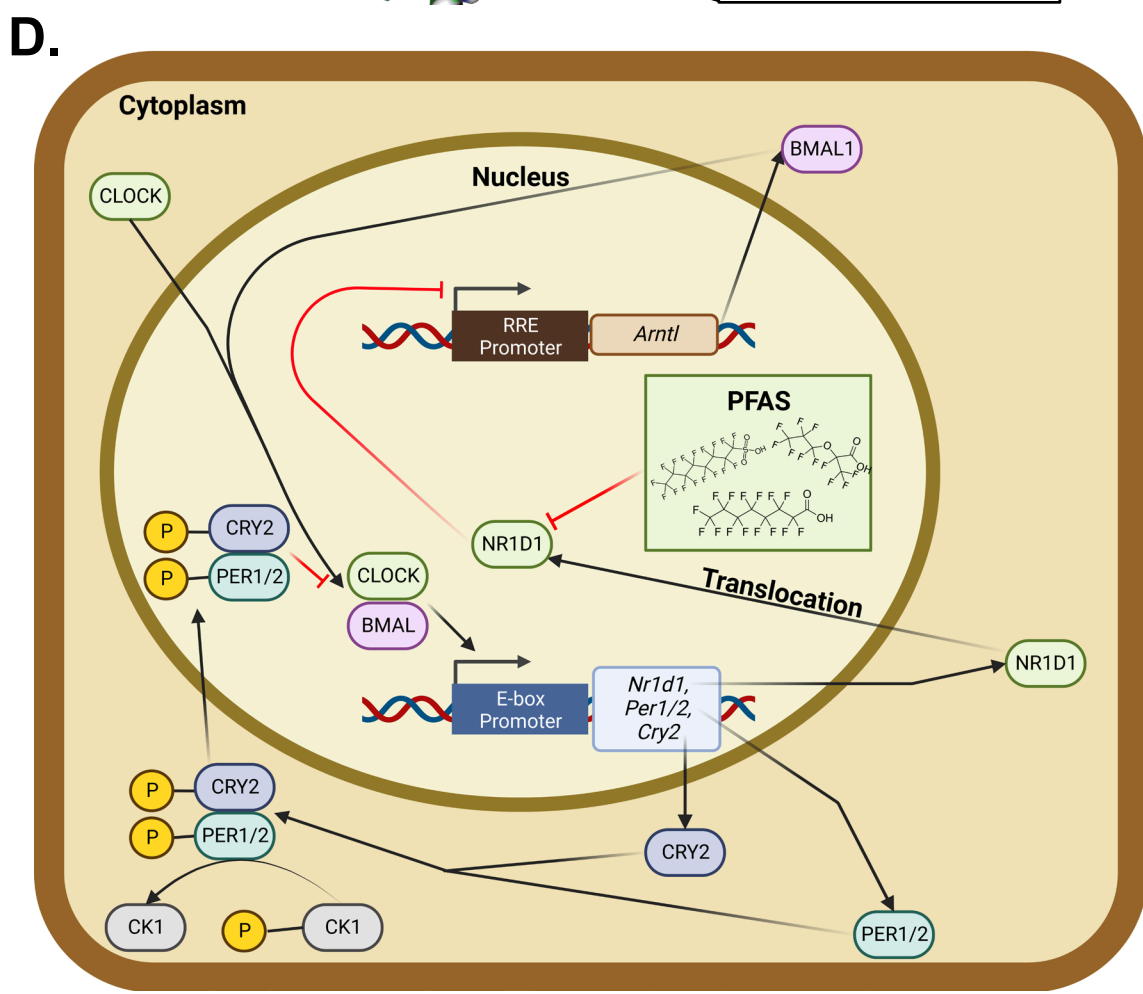
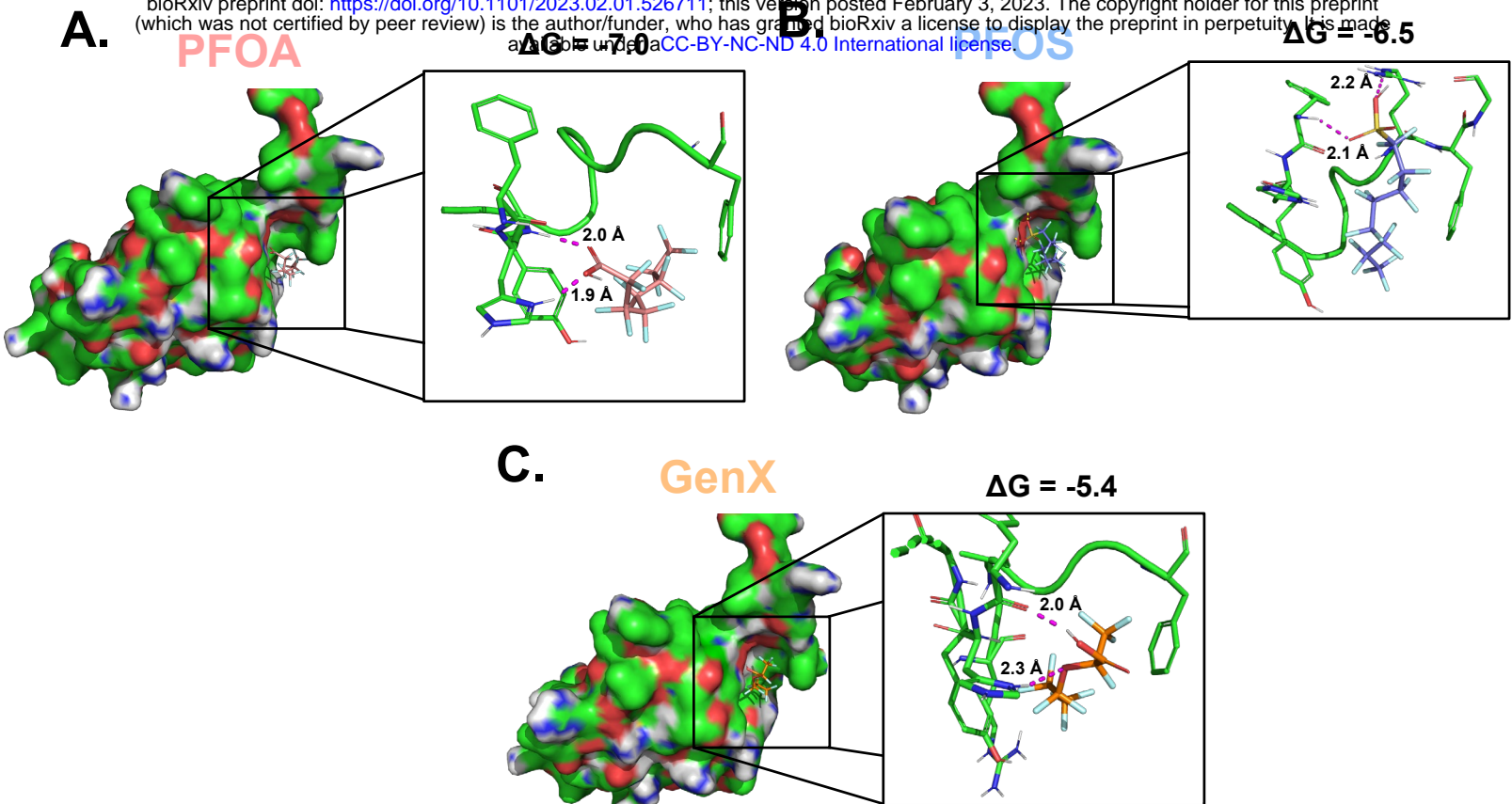
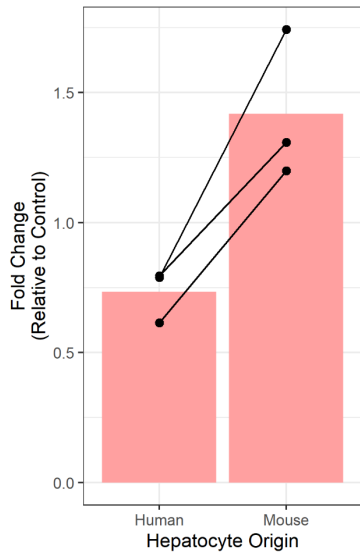


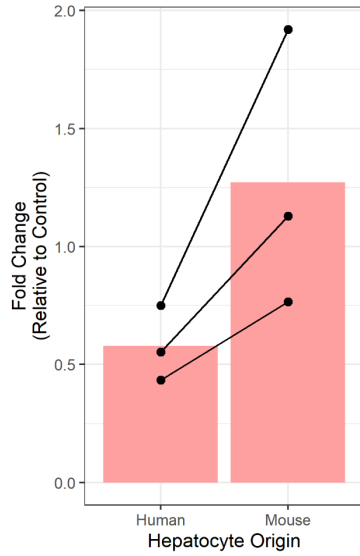
Figure 6

A.

**PFOA : Cpt1a
Species Comparison**

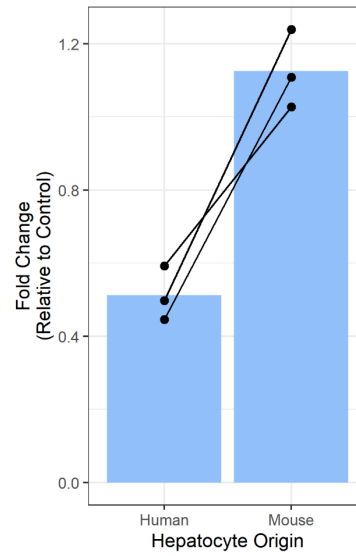


**PFOA : Hmgcs2
Species Comparison**

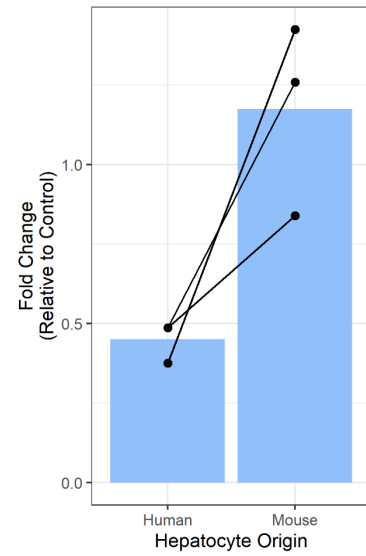


B.

**PFOS : Cpt1a
Species Comparison**

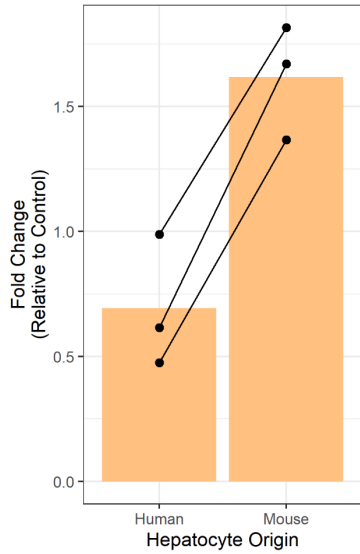


**PFOS : Hmgcs2
Species Comparison**



C.

**GenX : Cpt1a
Species Comparison**



**GenX : Hmgcs2
Species Comparison**

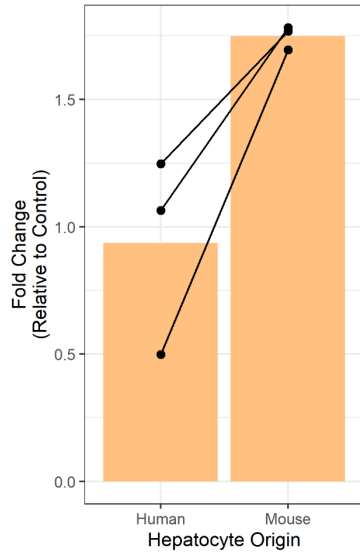


Figure S1

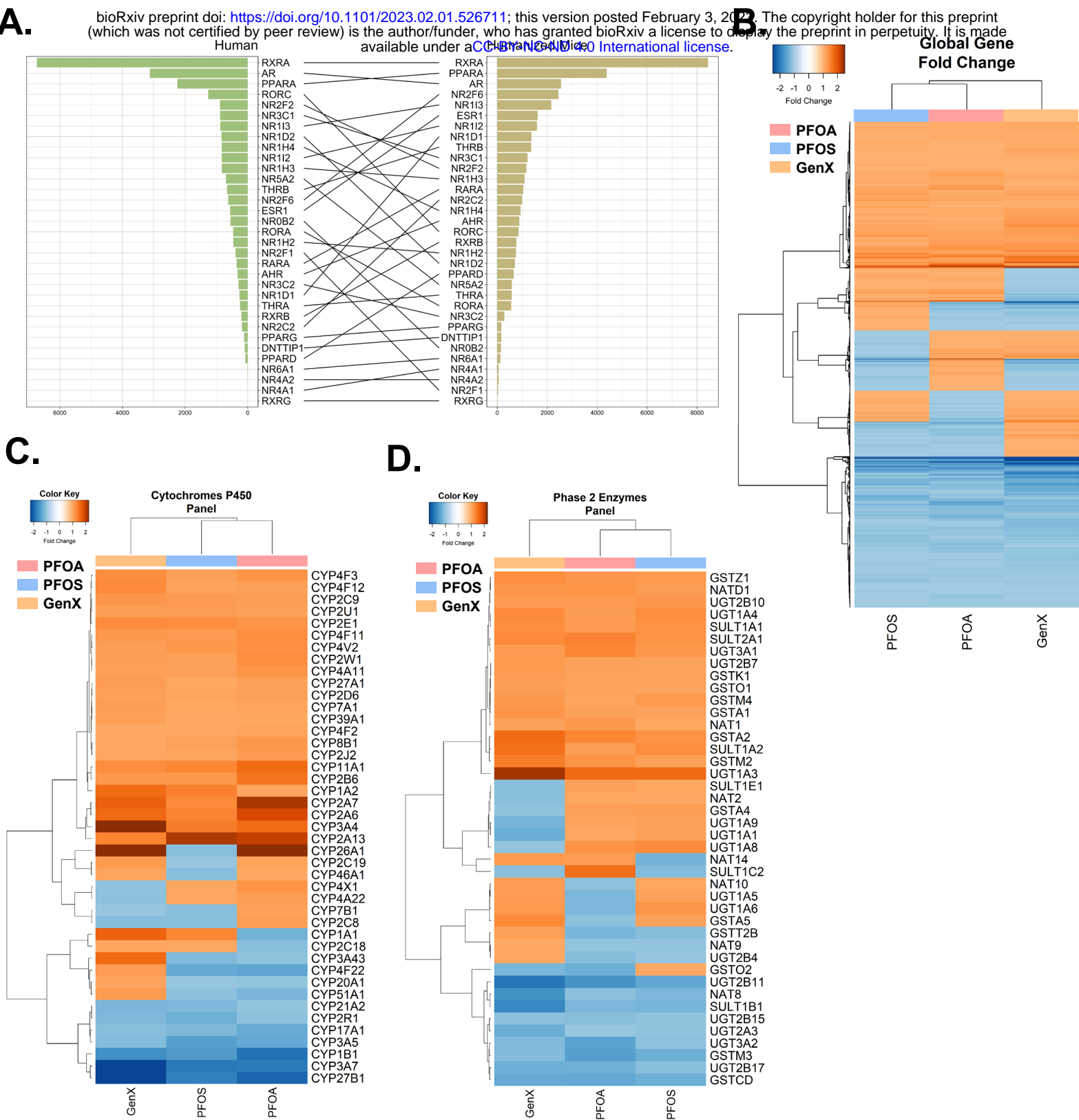


Figure S2

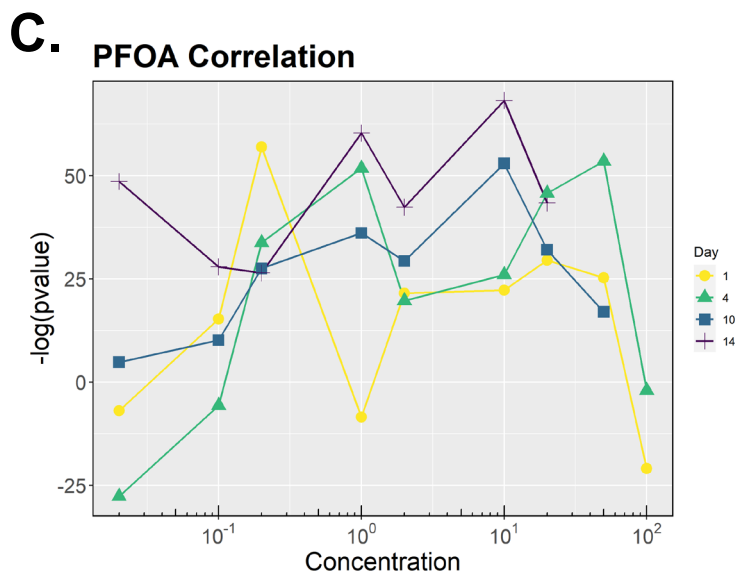
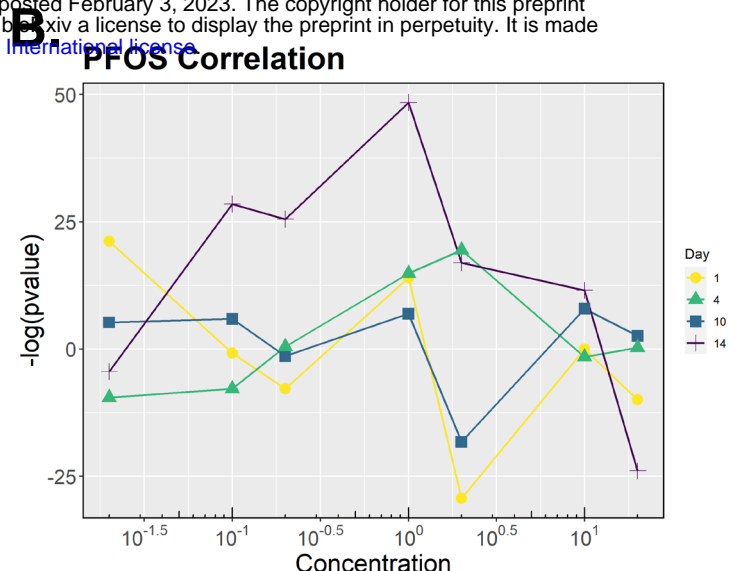
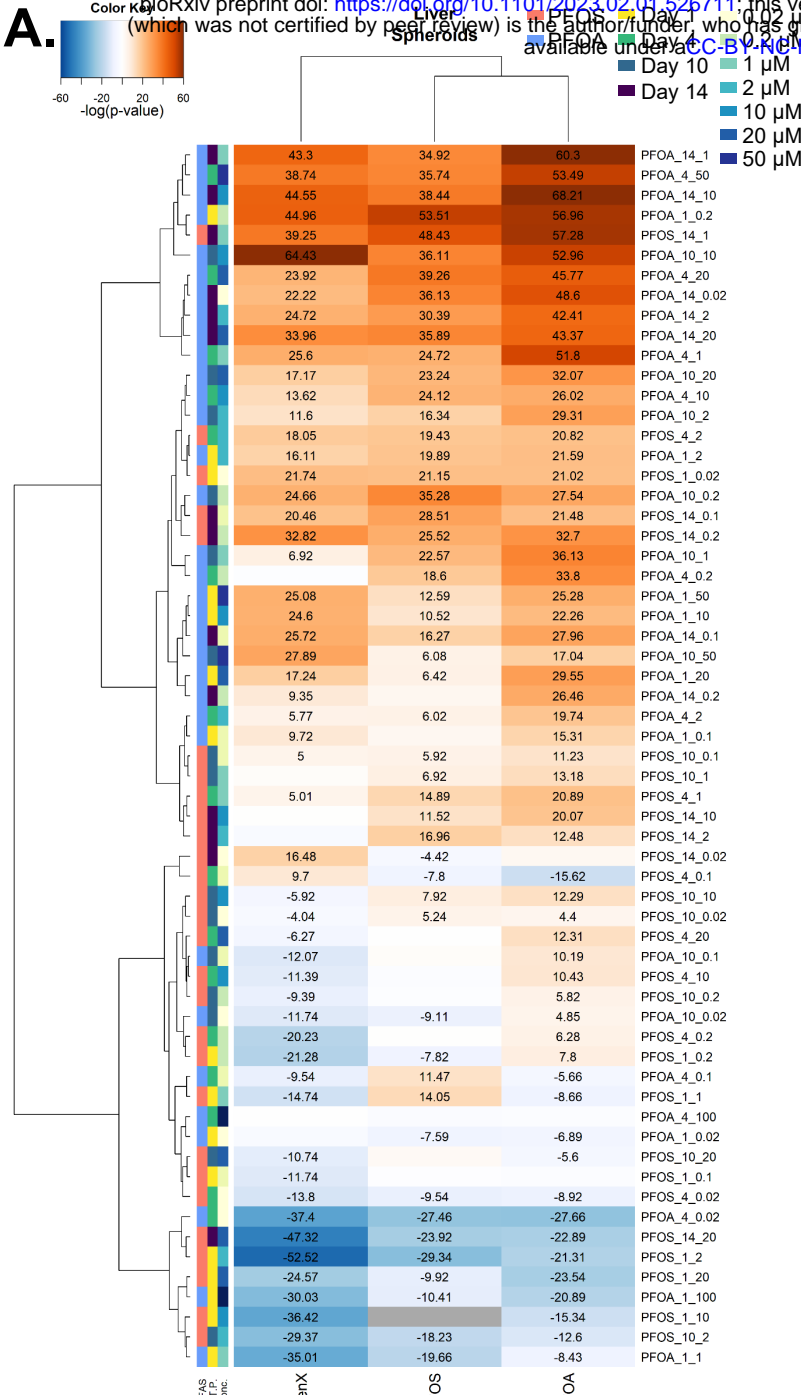


Figure S3

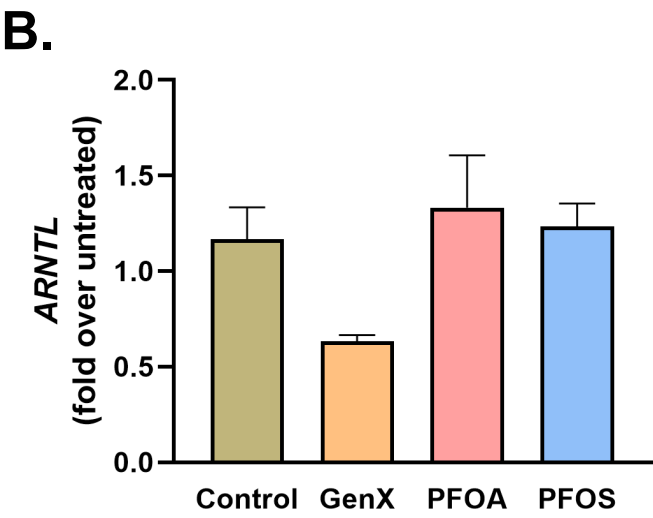
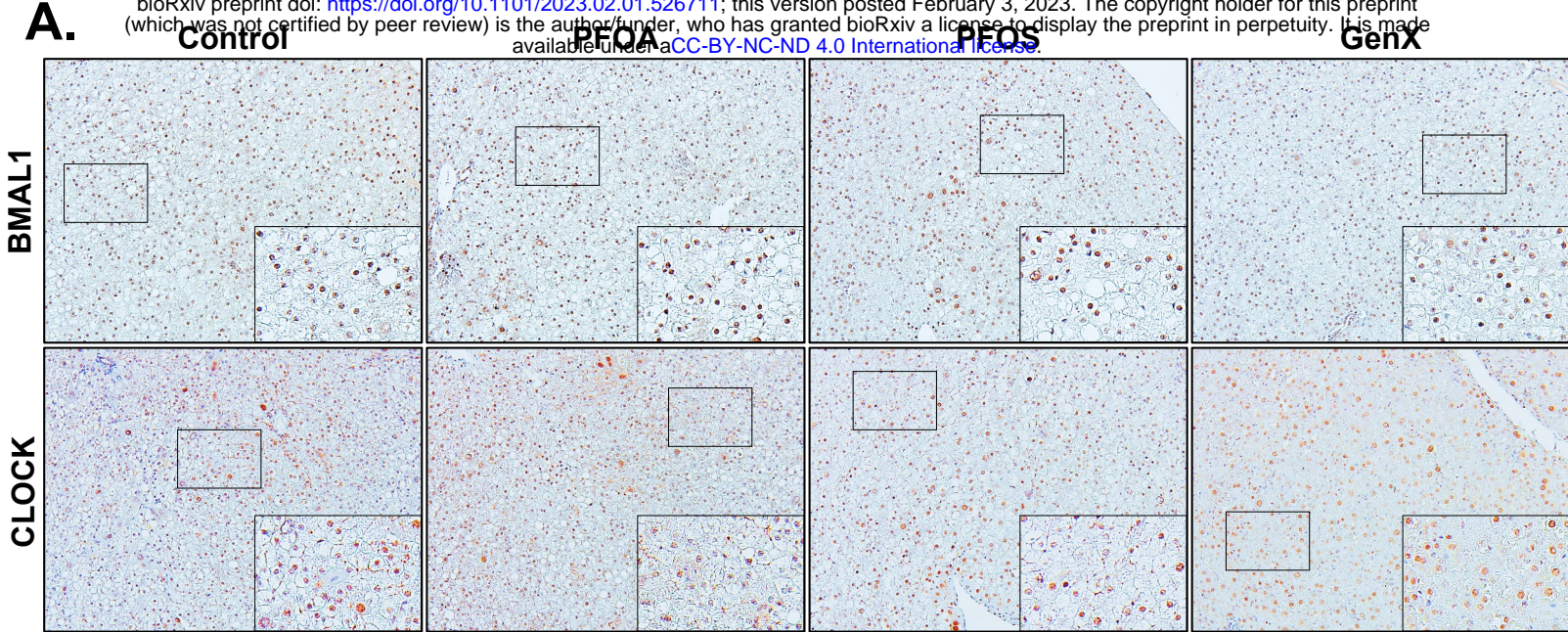


Figure S4